SCUOLA DI SCIENZE
Dipartimento di Chimica Industriale "Toso Montanari"

Corso di Laurea Magistrale in
Chimica Industriale
Curriculum: Advanced Spectroscopy in Chemistry
Classe LM-71 - Scienze e Tecnologie per la Chimica Industriale

Analysis of the high-resolution ro-vibrational spectrum of DC_3N in the far and mid infrared regions

CANDIDATE

Aleksandra Adamczyk

SUPERVISOR

Dr. Filippo Tamassia

CO-SUPERVISOR

Dr. Mattia Melosso

Session I

Academic Year 2019/2020

INDEX

ABSTRACT....2

1. INTRODUCTION....3

2. EXPERIMENTAL DETAILS....8
2.1 Synthesis of DC_3N....8
2.2 IR spectra recorded in Bologna....8
2.3 Far-Infrared (FIR) spectra recorded at the SOLEIL synchrotron facility....9

3. THEORETICAL ASPECTS....12
3.1 Rotational spectroscopy....12
3.2 Vibrational spectroscopy....14
3.3 Rotational structure in vibrational spectra....17
3.4 Ro-vibrational Hamiltonian for DC_3N....21

4. ANALYSIS OF THE SPECTRA....23
4.1 Assignment and analysis of the FIR region....23
4.2 The ν_7 fundamental and the $2\nu_7 \leftarrow \nu_7$ hot bands....26
4.3 The $\nu_5 \leftarrow \nu_7$ and $\nu_5+\nu_7 \leftarrow 2\nu_7$ bands....27
4.4. $\nu_6+\nu_7 \leftarrow 2\nu_7$ combination band and $4\nu_7 \leftarrow 2\nu_7$ hot band....29
4.5. Summary of the FIR region assignments....30
4.6 Vibrational stretching modes region....31
4.7 Global fit and derived spectroscopic constants....33

5. CONCLUSIONS....36

6. REFERENCES....37

APPENDIX....41

Abstract

Cyanoacetylene HC_3N is a molecule of great astronomical importance and it has been observed in many interstellar environments. Its deuterated form DC_3N has been detected in number of sources from external galaxies to Galactic interstellar clouds, star-forming regions and planetary atmospheres. All these detections relied on previous laboratory investigations, which however still lack some essential information concerning its infrared spectrum. In this project, high-resolution ro-vibrational spectra of DC_3N have been recorded in two energy regions: 150 – 450 cm^{-1} and 1800 – 2800 cm^{-1}. In the first window the $\nu_7 \leftarrow$ GS, $2\nu_7 \leftarrow \nu_7$, $\nu_5 \leftarrow \nu_7$, $\nu_5+\nu_7 \leftarrow 2\nu_7$, $\nu_6+\nu_7 \rightarrow 2\nu_7$, $4\nu_7 \leftarrow 2\nu_7$ bands have been assigned, while in the second region the three stretching fundamental bands ν_1, ν_2, ν_3 have been observed and analysed. The 150 – 450 cm^{-1} region spectra have been recorded at the AILES beamline at the SOLEIL synchrotron (France), the 1800 – 2800 cm^{-1} spectra at the Department of Industrial Chemistry "Toso Montanari" in Bologna.

In total, 2299 transitions have been assigned. Such experimental transition, together with data previously recorded for DC_3N, were included in a least-squares fitting procedure from which several spectroscopic parameters have been determined with high precision and accuracy. They include rotational, vibrational and resonance constants. The spectroscopic data of DC_3N have been included in a line catalog for this molecule in order to assist future astronomical observations and data interpretation.

A paper which includes this research work has been published (M. Melosso, L. Bizzocchi, A. Adamczyk, E. Cane, P. Caselli, L. Colzid, L. Dorea, B. M. Giulianob, J.-C. Guillemine, M-A. Martin-Drumel, O. Piralif, A. Pietropolli Charmet , D. Prudenzano, V. M. Rivillad, F. Tamassia, Extensive ro-vibrational analysis of deuterated-cyanoacetylene (DC_3N) from millimeter wavelengths to the infrared domain, Journal of Quantitative Spectroscopy and Radiative Transfer 254, 107221, 2020).

1. INTRODUCTION

My research project has been carried out in the field of infrared high-resolution spectroscopy and has the goal to assign and analyse some ro-vibrational bands of the linear molecule DC_3N, relevant to astrophysics and astrochemistry.

Spectroscopy is the science of light–matter interaction and is one of the most powerful scientific tools for studying nature. In the gas phase, it has been systematically used in studies of the sun, planets, stars, molecular clouds and for related laboratory investigation. The Universe is composed of 95.4% of dark matter and dark energy. The remaining small fraction is baryons contribution (consisting of atoms and molecules) which makes possible structures such stars, planets, and galaxies to form. Hydrogen and helium, the elements produced in the Big Bang are 98% of the total mass of baryons, while heavy elements have been synthesized little by little in stars and then distributed into the interstellar medium. Interstellar matter consists of gas and dust particles and it is not uniformly distributed over the galaxy but concentrated in clouds [1].

The beginning of astrophysical spectroscopy can be dated to the XIX century when dark lines in the solar spectrum caused by absorption of energy by atoms or ions in the solar atmosphere were discovered [2]. Further research of celestial bodies using spectroscopy connected astronomy with fundamental physics at molecular levels. The existence of molecules in interstellar clouds was established for the first time in 1940 [3] and it can be considered as the first important step of molecular astronomy.

The past decades have seen outstanding advances in the spectroscopy of astronomical sources, leading to expanded observational possibilities and interpretation analysis [4]. The detection of high-resolution astronomical spectra, in several ranges of the electromagnetic spectrum, led to developments in many areas of astrophysics, for example the derivation of isotope abundances in rapidly evolving stars, absorption spectroscopy of interstellar clouds and the composition of different objects [5]. The whole knowledge of astronomical species in the Interstellar Medium (ISM) comes from spectroscopic observations. Nowadays, one of the fundamental tasks of astrochemistry is to understand the stars and planets formation, the origin of the Solar System and the history of the Universe. The exploration of the formation processes and the chemical evolution of matter will eventually shed some light on the origin of life.

As far as the millimeter and submillimeter wavelengths are concerned, the biggest earth-based observatory is ALMA (Atacama Large Millimeter Array) observatory in Chile. Concerning the infrared regions, it is important to mention the Composite Infrared Spectrometer (CIRS), onboard the Cassini–Huygens spacecraft [6], with the aim to study the planet Saturn and its

system. New infrared data will be available once the James Webb telescope will be launched, at the end of 2021 [7].

Radio astronomy, namely the detection of pure rotational transitions, plays a crucial role in the observation of molecules in space and our understanding of interstellar chemical evolution and formation of planets. Also, the observation of rovibrational infrared and far-infrared spectra is of great importance for the identification of molecules in such remote environments. A renowned example of the Cassini probe, mentioned before, which explored in detail the chemistry of the atmosphere of Titan [6]. Infrared spectroscopy has the advantage, over pure rotational spectroscopy, to be able to detect molecules which lack a permanent dipole moment. To date, over 200 molecules have been detected in the interstellar medium (ISM) or circumstellar shells. Most new molecule detections (~80%) have been made using radio astronomy techniques, because interstellar matter is at temperature of few Kelvin and thus emits radio-waves only [8]. The phenomenon for which matter emits at a nonzero temperature is called thermal emission. In general, its intensity depends on the composition of material as well as its temperature and carries information about emission sources, for example the chemical composition and relative molecular abundances.

Each year, new molecules are discovered in space and the study of interstellar molecules has helped already, for example, to clarify the evolutionary stages of star formation in the Milky Way [9]. But despite many new molecular detections, the number of unidentified molecular spectral features is huge. My research work conducted for this thesis is the analysis of some ro-vibrational bands of deuterated cyanoacetylene, a very important astrochemical molecule and a member of the cyanopolyynes family. The spectra analyzed have been recorded with a Fourier transform infrared (FTIR) spectrometer at the SOLEIL synchrotron facility in Paris in the far-infrared region and with and at the Department of Industrial Chemistry "Toso Montanari" in Bologna in the infrared region.

Polyyines and cyanopolyynes, linear carbon chain species with formula $C_{2n+2}H_2$ and $HC_{2n+1}N$, respectively, represent important classes of polyatomic molecules identified in space. In the interstellar medium (ISM), chains up to n = 11 have been detected [10]. Various mechanisms have been proposed for the synthesis of $HC_{2n+1}N$ molecules in cold dark cloud cores. According to J. C. Loison [11] cyanopolyynes are produced mostly through C and C+ induced reactions, which proceed until most of the gas-phase carbon is locked in CO and then depleted onto dust grains. The elementary reactions of atomic carbon lead to an increase in the size of the chains,

the reactions of nitrogen act to reduce it by breaking carbon-carbon bonds producing CO and CN radicals. Further reactions may lead to cyanopolyynes containing many carbon atoms.

In this project, the deuterated form of cyanoacetylene has been studied. The detection of rare isotopic molecular species provides in fact important information about the physical and chemical properties of astronomical objects, as well as on their evolutionary stage. In the absence of chemical fractionation (a process by which chemical reactions produce abundance ratios among isotopologues different from the actual elemental abundance ratios) the isotopologues can be used to determine elemental abundance ratios such as D/H (estimated to be 1.6×10^{-5}) in different places in the universe [12]. Deuteration of organic molecules in the interstellar medium is a powerful tracer of the history of star-forming regions. In prestellar cores, at low temperatures and high densities, more H_3^+ molecules can be found, because of the depletion of CO molecules, the main destroyer of H_3^+, onto the surface of dust grains. Intensified reaction of H_3^+ with HD, abundant in molecular clouds, produces H_2D^+, which transfers the deuterium to different molecules by further reactions, resulting in a significant increase in deuterium fractionation [13]. The increase in the deuteration in cold, prestellar cores leads to an overall enhancement of atomic deuterium in the gas phase. After reaching the surface of dust grains, deuterated molecules can participate in the deuterium fractionation of molecules already formed on these grains, in particular of the complex organic molecules. The ratio of one species containing deuterium to its counterpart containing hydrogen is a relic of the conditions that were prevailing in earlier, colder stages and can be used as ~~a~~ tracer of the evolution of the star-forming cores [14].

The widespread presence of the cyanoacetylene molecule in interstellar space has made HC_3N a molecule of great astronomical interest [15]. This linear carbon chain molecule was found to be an abundant species in a variety of astronomical object and as the simplest member of the family of cyanopolyynes became an important species in the study of interstellar molecular synthesis [16]. Cyanoacetylene has been identified in a large variety of astronomical objects like comets, the interstellar medium and star forming regions, mainly by radio observations [17].

The deuterated form of cyanoacetylene has been observed for the first time towards the Taurus Molecular Cloud (TMC-1) in 1980, where HC_3N emission is strong and the longer cyanopolyamines have also been detected. Comparison of DC_3N with HC_3N indicated then that in TMC-1 this species is formed by gas-phase ion molecule reaction [18]. DC_3N was also observed towards several other dark clouds (TMC-2, TMC-1C, L1498, L1514) finding the

enhanced ratio D/H of deuterated cyanoacetylene in the range 0.03-0.13. In the protostellar phase, DC_3N has been detected towards several sources: the solar-type prostar IRAS 16293-2422 [19], the low-mass star forming regions L1527 [20] and Chamaeleon MMS1 [21], and the prostar SVS13-A [22] with values of deuterium fractionation $\sim 0.03-0.4$. DC_3N has been tentatively reported also in the high-mass star-forming regions Orion KL [23] and Sagittarius B2 [24]. In these regions, the deuterium fractionation is not as effective as in dark clouds, thus preventing a strong enhancement above the deuterium cosmic abundance. Recently, DC_3N has been detected in some low-mass cores and in a sample of 15 high-mass star-forming cores [25]. The latter work suggests that DC_3N is enhanced in the cold and outer regions of star-forming regions, likely indicating the initial deuteration level of the large-scale molecular cloud within which star formation takes place.

The detection and determination of the mean abundance of molecules by spectroscopy are based on the knowledge of their spectroscopic line positions and intensities. However, there is a general lack of appropriate experimental data for DC_3N [26].

The first microwave studies of deuterated cyanoacetylene dates back to 1978 by P.D.Mallison and R. Zafra [27]. In this work, the first precise measurements of pure rotational transitions in the ground and ν_4, ν_6, ν_7 vibrational excited states have been performed. Ten years later, 12 excited vibrational states were observed and analysed and further studies allowed the determination of several effective molecular parameters [28]. The improvement of the sensitivity and spatial resolution of radiotelescopes triggered a number of further laboratory studies to provide the necessary data to identify the molecular spectral features in Space. In 2008, the investigation of the rotational spectrum of DC_3N has been extended for the ground state and the $v_7 = 1$ lowest excited vibrational state [29]. Concerning the infrared spectrum of DC_3N, intensities of three bending fundamentals modes were measured in 1982 [30] and IR vibrational studies in medium resolution were also performed during the last years [31]. The experimental position of all fundamentals, with few overtone and combination bands, have been determined from a low resolution (0.5 cm^{-1}) study [26]. The band centers of the three stretching modes of DC_3N (ν_1, ν_2, and ν_3) has been determined [32] and the ν_7 fundamental mode was analyzed together with the bands $\nu_6 - \nu_7$, $\nu_5 - \nu_7$, $\nu_4 - \nu_6$, and their hot-bands [31].

As far as the parent species HC_3N is concerned, the most exhaustive work is a global analysis of all the existing pure rotational and high-resolution IR measurements [33].

Theoretical aspects of DC_3N spectroscopy are described in detail in Section 3 with some basic knowledge of molecular spectroscopy. Section 2 introduces the experimental setup and the sample specification. Investigations, analysis and interpretation of ro-vibrational spectrum of DC_3N are presented in the Section 4. The last part of the work contains summary and conclusions with possible perspectives. In appendix, the spectroscopic parameters obrtained from the global fit are listed.

2. EXPERIMENTAL DETAILS

2.1 Synthesis of DC_3N

The DC_3N sample was synthesized in Rennes with the procedure described in Ref. [26]. Cyanoacetylene was obtained according to the procedure introduced in 1920 by Moureu and Bondgrand [34] and then modified by Miller and Lemmon in 1967 [35]. Methyl propiolate ($HC \equiv CCOOCH_3$) with > 98% purity was purchased from TCI-Europe and it was added dropwise to liquid ammonia resulting in a 100 % conversion to propiolamide ($HC{\equiv}CCONH_2$). The propiolamide was mixed with phosphorous anhydride (P_4O_{10}) and then calcined white sand. The system was heated up to 470 K over 2 hours while connected to a liquid nitrogen-cooled trap where pure cyanoacetylene was collected.

Cyanoacetylene (HC_3N, 3 g), deuterated water (D_2O, 4 mL) and potassium carbonate (K_2CO_3, 50 mg) were mixed under nitrogen and the biphasic mixture was then energetically stirred for 20 min at room temperature. In the next step, the system was adapted to a vacuum line with two traps. Water was blocked in a first 220 K trap and partially deuterated cyanoacetylene was condensed in a 77 K cooled trap. The whole sequence was repeated three times by addition of D_2O and K_2CO_3 to the partially deuterated cyanoacetylene. The residual D_2O was removed by vaporisation on P_4O_{10} and the product was finally condensed in a trap cooled to 150 K. DC_3N with an isotopic purity greater than 98 % was obtained in a 67 % yield.

2.2 IR spectra recorded in Bologna

The infrared spectra in the 1900 – 2800 cm^{-1} range were recorded in Bologna using a Bomem DA3.002 Fourier Transform infrared spectrometer (FTIR). The spectrometer was equipped with a Globar source (silicon carbide bar), a KBr beamsplitter and a liquid nitrogen cooled HgCdTe detector. In the spectrometer the output radiation is firstly focused into an iris and then, through a series of mirrors, hits a beamsplitter. A 8 m pathlength white-type multi-pass absorption cell was used. The pressures adopted were 16 and 32 Pa. The instrumental resolution of the recorded spectra was 0.004 cm^{-1}. Several hundred scans were co-added to improve the signal-to-noise ratio of the spectra. The scheme of the Bomem DA3.002 FT-IR spectrometer is shown in the Figure 2.1. The spectra were calibrated by means of the residual H_2O and CO_2 present in the spectra [36, 37].

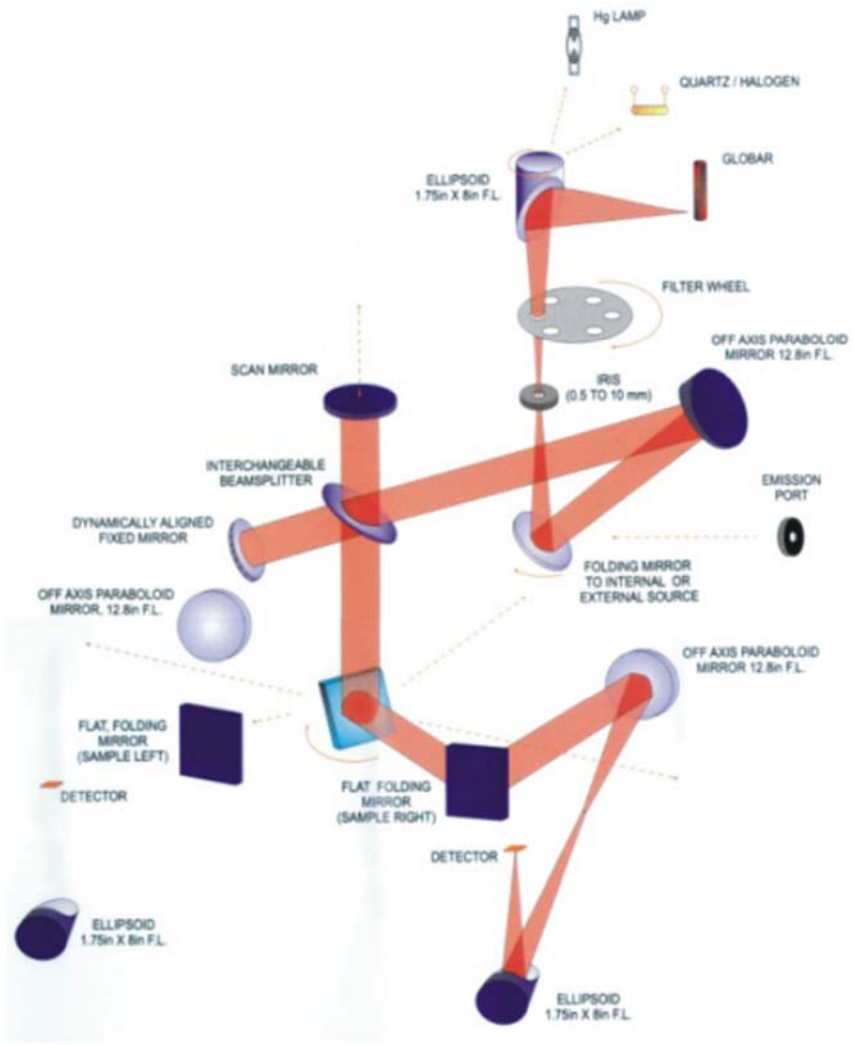

Figure 2.1. Scheme of Bomem DA3.002 FT-IR spectrometer at Dipartimento di Chimica Industriale "Toso Montanari".

2.3 Far-Infrared (FIR) spectra recorded at the SOLEIL synchrotron facility

The far infrared spectra were recorded at the AILES Beamline at the SOLEIL Synchrotron facility in France. This beamline, taking advantage of the natural synchrotron high brilliance, is operating in a wide variety of research topics and provides high resolution spectroscopic data [38]. The spectral range goes from the MIR to the FIR domains, with the best performances below 1000 cm^{-1} and a maximum resolution of 0.0008 cm^{-1}. The FIR spectrum of DC_3N was recorded using a Bruker IFS 125 FT interferometer [38] and a white-type multipass absorption cell. The absorption cell's optics were set to obtain a 151.75 m long absorption path [39] and

the cell was isolated from the interferometer by two polypropylene windows (See Figure 2.2). For the experiment, a Mylar-composite beamsplitter and a 4 K cooled Si-bolometer detector were used. The interferometer was continuously evacuated to 0.01 Pa, limiting the absorption of atmospheric water. Vapor pressure of DC_3N was injected into the absorption cell at 25 and 100 Pa pressures.

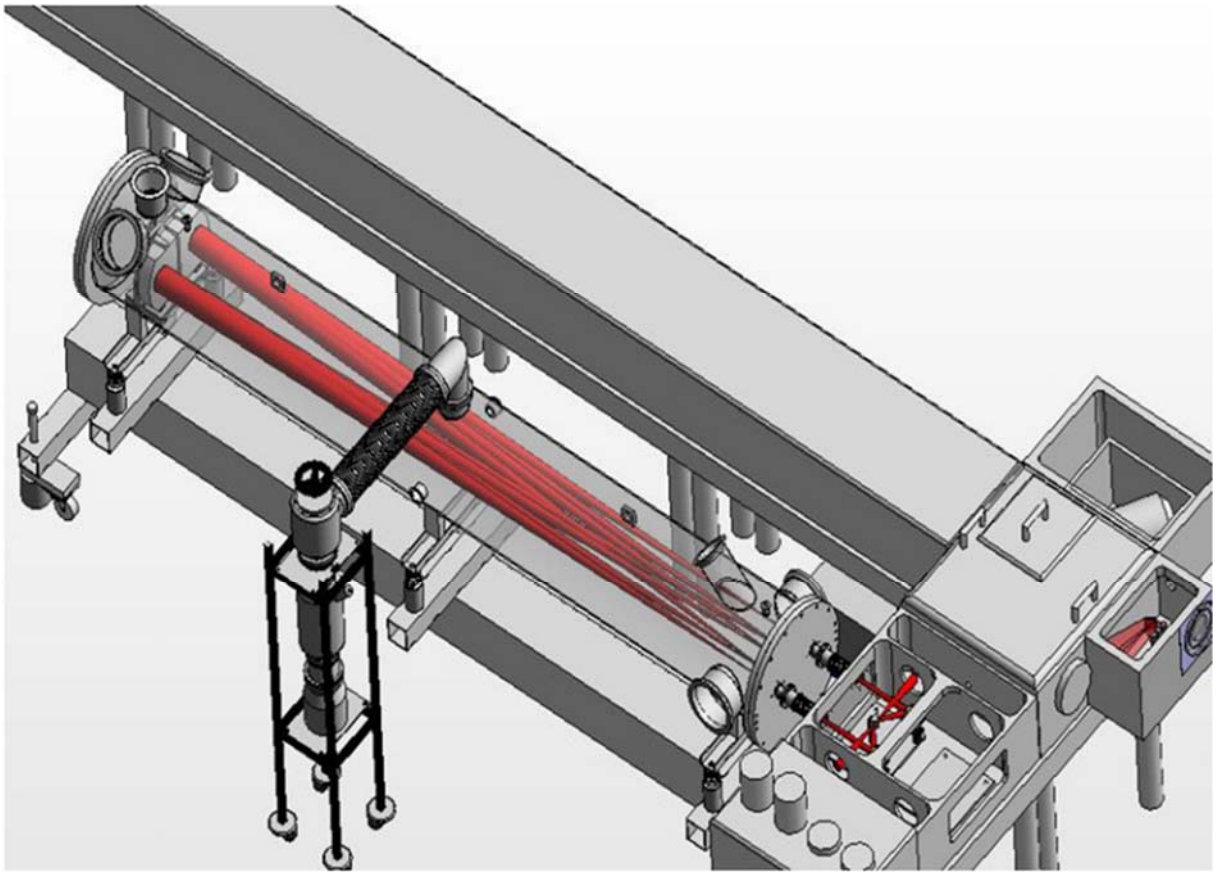

Figure 2.2. Experimental set-up at the AILES beamline of the SOLEI synchrotron.

The spectrum covers the range 70–500 cm^{-1} and consists of the co-addition of 380 scans recorded at 0.00102 cm^{-1} resolution. In Figure 2.3, the obtained transmittance spectra of DC_3N is showed.

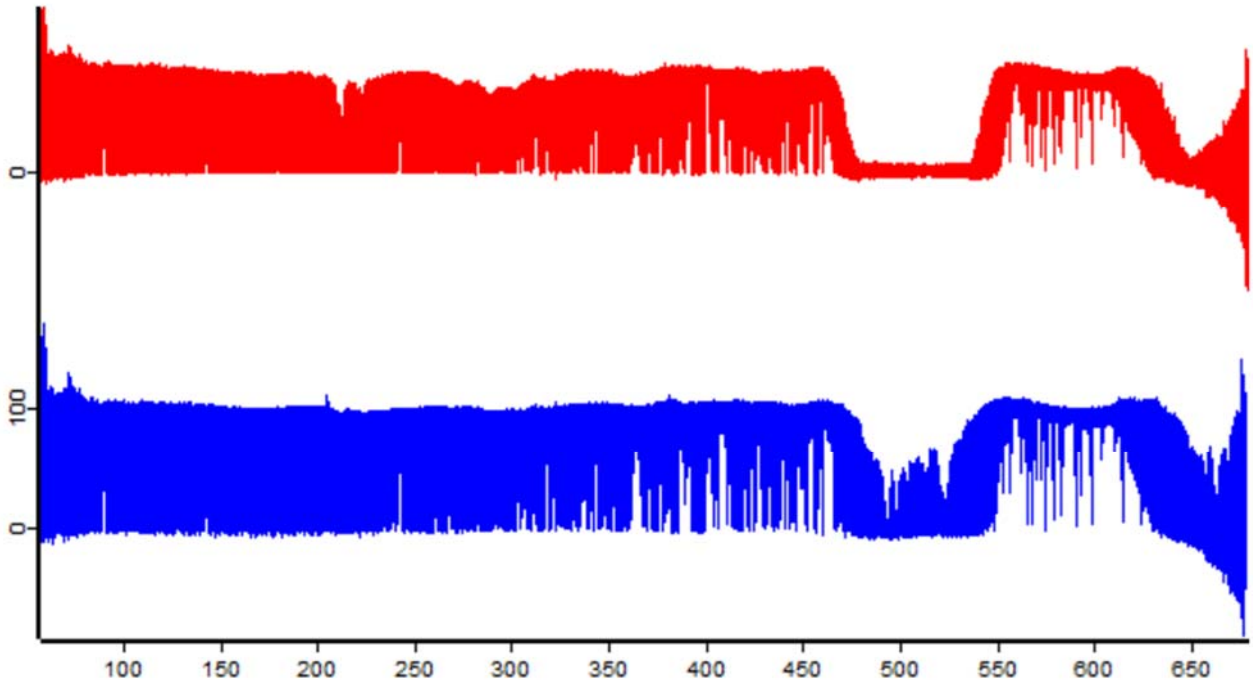

Figure 2.3. Transmittance spectra of DC_3N recorded at the AILES beamline of the SOLEI synchrotron with 25 Pa (in blue) and 100 Pa (in red).

All the spectra have been calibrated by referencing ro-vibrational transitions of H_2O and CO_2 absorption lines whose reference were taken from literature [40, 41] and from HITRAN [37] database.

3. THEORETICAL ASPECTS

DC_3N is a linear molecule with structural formula D ─ C ≡ C ─ C ≡ N. I will briefly summarize the features of the rotational and vibrational spectra for a general linear molecule. The description of the energies, matrix elements and selection rules will be completed with the inclusion of some special interactions, called resonances, which apply only to DC_3N.

3.1 Rotational spectroscopy

Rotational spectroscopy detects the transition between the quantized energy levels of a molecule rotating freely in space. Pure rotational spectroscopy transitions are generally observed as resolved transitions for molecules in the gas phase, the only state of matter in which molecules can rotate freely and can be considered isolated to a good approximation (the effects of collisions are however observed). The microwave region is, in general, the portion of the electromagnetic spectrum explored by these transitions. From the observed rotational spectra, a set of molecular spectroscopic parameters can be derived with high precision. The energy levels spacing depends mainly on the mass distribution within the molecule, namely its geometry and the type of atoms present in the molecule. This is what makes rotational spectroscopy a powerful technique to determine structural parameters.

The total energy for any N-particle system can be separated into the sum of the kinetic energy of motion of the overall system and the potential energy. The simultaneous description of the motions of the nuclei and electrons is not trivial. Since nuclei are much heavier than electrons and they move much slower, the Born-Oppenheimer approximation can be applied in order to treat them separately. Such approximation allows a relatively straightforward treatment of the nuclear motion: the overall rotation of the molecule and the molecular vibrations. The energies related to the nuclei can be also separated in rotational, vibrational and nuclear spin orientation degrees of freedom. Molecular energies for different types of motion can be treated separately and conveniently.

In general, the kinetic energy of a body rotating at an angular velocity ω is given by equation:

$$E_{kin} = \frac{1}{2}\omega \mathrm{I} \omega \tag{1}$$

where *I* is the tensor of inertia which has the form:

$$I = \begin{pmatrix} I_{xx} & I_{xy} & I_{xz} \\ I_{yx} & I_{yy} & I_{yz} \\ I_{zx} & I_{zy} & I_{zz} \end{pmatrix} \tag{2}$$

The diagonal elements of this tensor are called moments of inertia about the X, Y and Z axis while the off-diagonal elements are products of inertia. Since the tensor is real and symmetric ($I_{ij} = I_{ji}$), one can always find some rotation coordinates system such that in the new system the tensor *I* is diagonal. So, in the new coordinates system, the tensor of inertia is written:

$$I = \begin{pmatrix} I_{aa} & 0 & 0 \\ 0 & I_{bb} & 0 \\ 0 & 0 & I_{cc} \end{pmatrix} \tag{3}$$

Since $I_z = 0$, $I_x = I_y = I$ (assuming z=a, x=b, y=c) for a linear molecule and symbol *L* is used to represent total angular momentum $L = I * \omega$. The expression for the rotational kinetic energy of a rigid rotor can therefore be written as:

$$E_{kin} = \frac{L^2}{2I} \tag{4}$$

In quantum mechanical terms, this is expressed through the Hamiltonian:

$$\widehat{H} = \frac{\widehat{L^2}}{2I} \tag{5}$$

The corresponding rotational energy levels, obtained by solving the Shrödinger equation, are given by the expression:

$$E_{rot} = \frac{1}{2I} J(J+1)\hbar^2 = BJ(J+1) \tag{6}$$

where J is rotational quantum number and B is rotational constant $B = \frac{\hbar^2}{2I} = \frac{\hbar^2}{2\mu r_e^2}$, where r_e is the equilibrium bond length [34], if the equilibrium position is considered.

The intensity of a pure rotational transition is determined by the dipole transition moment:

$$M = \int \psi_{J'} \mu \psi_J d\tau \tag{7}$$

If the molecule has no permanent electric dipole moment, rotational transitions are not allowed [43]. The selection rule $\Delta J = \pm 1$ for a linear molecule results in transitions with frequencies:

$$v = B(J+1)(J+2) - BJ(J+1) = 2\mathrm{B}(J+1) \tag{8}$$

A chemical bond is not rigid. In fact, when a molecule rotates, the atoms experience a centrifugal force and the length of chemical bond increases. This force is balanced by the Hooke's law restoring force. This behaviour is considered by introducing a centrifugal distortion constant D as follow:

$$E_{rot} = BJ(J+1) - D[J(J+1)]^2 \tag{9}$$

As a first approximation, a relation between D and ω (the frequency of the fundamental harmonic vibration) can be established:

$$D = \frac{4B^3}{\omega^2} \tag{10}$$

and the transition energy becomes:

$$v_J = E_{J+1} - E_J = 2B(J+1) - 4D(J+1)^3 \tag{11}$$

More centrifugal distortion terms can be added to Eq. (9), like *H*, *L*, ..., which multiply higher powers of *[J(J+1)]*.

3.2 Vibrational spectroscopy

Vibrational spectroscopy detects transitions between the quantized energy levels associated

with the molecular vibrations. The transitions are detected by absorption or emission spectroscopy generally in the infrared region of the electromagnetic spectrum. The knowledge of the vibrational spectroscopic constants allows to obtain the value of the bonds force constant and to estimate their dissociation energy. It also provides a useful tool for identifying the characteristic functional groups within a molecule.

The quantum model for the description of the vibrational energy levels is the harmonic oscillator. According to Hooke's Law, when a particle is displaced from its equilibrium position r_e, it is subjected to a restoring force F proportional to the displacement $r-r_e$:

$$F = -k(r - r_e) \tag{12}$$

where k is the force constant in Nm^2. The force is linked to the potential energy, in fact:

$$F = \frac{-dV}{dr} \tag{13}$$

and after integration:

$$V = \frac{1}{2}k(r - r_e)^2 \tag{14}$$

The Shrödinger equation for such motion is expressed as below:

$$\widehat{H_{vib}}\psi(r) = \frac{-\hbar^2}{2\mu}\frac{d^2\psi(r)}{dr^2} + V(r)\psi(r) = E_{vib}\psi(r) \tag{15}$$

with eigenvalues:

$$E_{har} = h\upsilon_e(v + \frac{1}{2}) \tag{16}$$

where subscript *har* means: harmonic oscillator; h is Planck constant, υ_e is the harmonic frequency in Hz, and v is vibrational quantum number.

The harmonic oscillator model is clearly unrealistic for a real molecular potential energy, as it describes bonds which never break. A more realistic and widely used model for molecular

potential energy functions is the Morse function:

$$V(r) = D_e(1 - e^{-\beta(r-r_e)})^2 \tag{17}$$

where: D_e is the bond dissociation energy; r_e is the equilibrium bond length, β is a parameter related to force constant k, describing the stiffness of small amplitude vibration near the minimum.

The Shrödinger equation for a Morse potential may be solved analytically to give an exact closed form expression for its vibrational energy levels:

$$E_{Mo}(v) = G(v) = \omega_e(v + \tfrac{1}{2}) - \omega_e x_e(v + \tfrac{1}{2})^2 \tag{18}$$

In the above equation, $\omega_e x_e$ in the first anharmonicity constant. A general description of the potential energy is usually obtained with a power series of the vibrational coordinates, which yields vibrational energies as powers of (v+1/2).

So far, we have described the vibrational energy of a one-dimensional oscillator, either harmonic or anharmonic. At a molecular level, this is appropriate only for diatomic molecules. For polyatomic linear molecules, all the vibrational modes contribute to the total vibrational energy. The description of the derivation of the vibrational modes, called normal modes, will not be reported here. For a molecule with N atoms, the number of vibrational normal modes is 3N-6 for bent molecules and 3N-5 for linear molecules. Equation (19) therefore becomes, for linear molecules:

$$E_k(v) = \sum_{k=1}^{3n-5}(v_k + \tfrac{d_k}{2})\,\omega_k - \sum_{j\geq k}^{3n-5}(v_j + \tfrac{d_j}{2})\,(v_k + \tfrac{d_k}{2})x_{jk} \tag{19}$$

where E_k is the energy for k^{th} vibration of the molecule and x_{jk} are anharmonicity constants. The d_j, d_k constants are the degeneracy factors, equal to 1 for the stretching modes and 2 for the bending modes. It is important to point out that Eq. (19) reports only the first anharmonicity constants but, in general, other higher-order terms can be added.

A transition between two vibrational levels is possible if the transition moment is non vanishing.

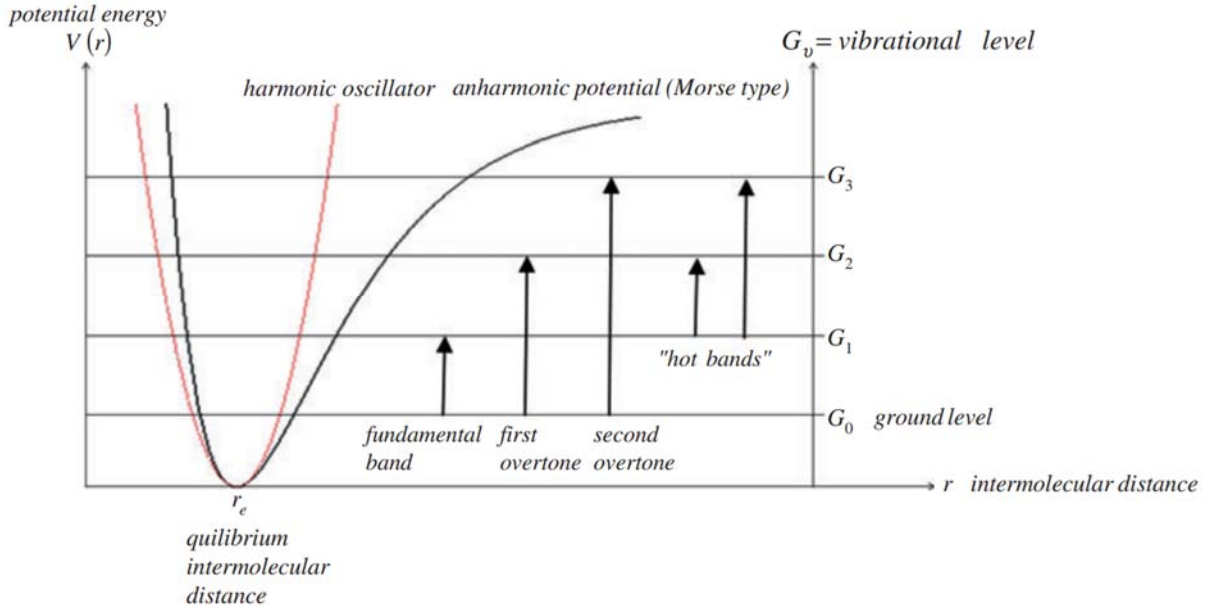

Figure 3.1. Vibrational levels and transitions. The harmonic oscillator and the Morse potential energy functions are shown [44].

$$M = \int \psi_{v'}{}^{*} \mu \psi_{v''} d\tau \tag{20}$$

In the case of the anharmonic oscillator, the selection rules are Δv = ±1, ±2, ±3, ±4 ... Simultaneous excitations of different vibrational modes are allowed. It is important to point out that, in the case of vibrational transitions, molecules are not required to have a permanent dipole moment but a variation of the dipole moment during the excitation.

In Figure 3.1 the main transitions in a vibrational spectrum are shown. The v = 1 ← 0 is known as the fundamental vibration. Other transitions originating in v = 0 are known as overtones. All transitions among higher vibrational levels are known as hot bands.

3.3 Rotational structure in vibrational spectra

In general, molecules vibrate and rotate at the same time, thus giving rise to vibration-rotation spectra. In vibration–rotation spectroscopy we observe transitions between stacks of rotational energy levels associated with two different vibrational levels. If, for simplicity, we limit our description to the first anharmonicity term and to the first centrifugal distortion term of a diatomic molecule, the total ro-vibrational energy can be written:

$$E(v,J) = E_{vib}(v) + E_{rot}(J) = \omega_e(v+\tfrac{1}{2}) - \omega_e x_e(v+\tfrac{1}{2})^2 + B_v J(J+1) - D_v[J(J+1)]^2 \tag{21}$$

The observed rotational transitions associated with a vibrational transition follow the selection rules $\Delta J = 0, \pm 1$. The groups of transitions corresponding to such selection rules are called: R branch ($\Delta J = +1$) P branch ($\Delta J = -1$) and Q branch ($\Delta J = 0$), as shown in Figures 3.2 and 3.3.

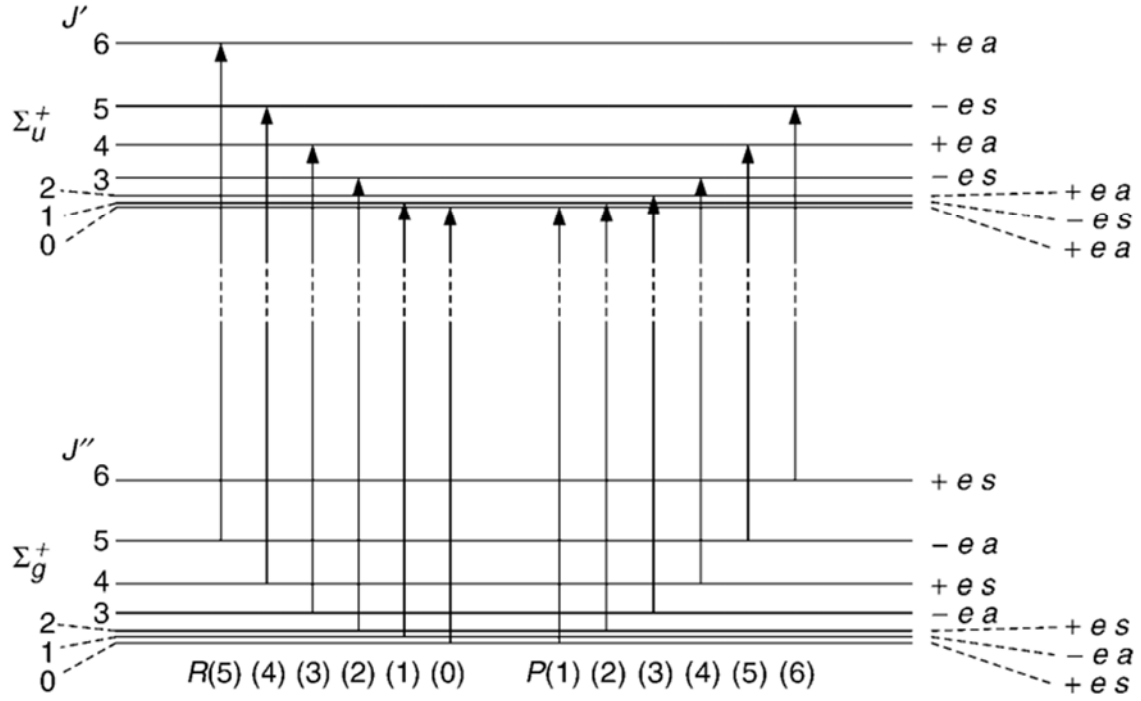

Figure 3.2. Rotational transitions accompanying a Σ-Σ infrared vibrational transition in a linear polyatomic molecule with a centre of symmetry. For molecules without a centre of symmetry, the g and u subscripts and s and a label should be dropped [45].

The resulting spectrum shows P- and an R-branches with lines separated by about 2B, where B is an average rotational constant for the two vibrational states, and a spacing of about 4B between R(0) and P(1).

The selection rule $\Delta J = 0$ applies only to transitions which involve some excitations of the bending states. This is a consequence of the fact that bending modes produce a vibrational angular momentum

$$L_z = \hbar l \tag{22}$$

where l is the associated quantum number, and is related to the corresponding vibrational quantum number v_i for the bending mode i by the equation:

$$l_i = v_i, v_i-2, \ldots -v_i \tag{23}$$

The presence of this additional angular momentum is responsible for the splitting of rotational levels in vibrational bending states called *l-doubling*. The ±*l* degeneracy is removed because of the Coriolis interaction between rotational and vibrational motions. The split energy levels are indicated with the *e* ed *f* labels.
If $l = 1$, the magnitude of such splitting is:

$$\Delta E_{(l)=1} = \left(\frac{q_i}{2}\right)(v_i + 1)J(J+1) \tag{24}$$

where q_i is the spectroscopic parameters that determines the energy separation. The expression of the rotational energy is modified accordingly:

$$E_r = BJ[(J+1) - l^2] - D(J(J+1) - l^2)^2 + H(J(J+1) - l^2)^3 + L(J(J+1) - l^2)^4 \pm \frac{q_i}{4}(v_i + 1)J(J+1) \tag{25}$$

The total quantum number J cannot be lower than *l*, therefore $J \geq l$. For high values of J, it is necessary to introduce additional terms that account for the centrifugal distortion effects. The *l-doubling* parameter q_i is better described by a new form, which includes a centrifugal distortion dependence:

$$q_i = q_{i0} - q_{iJ}J(J+1) + q_{iJJ}\big(J(J+1)\big)^2 \ldots \tag{26}$$

The vibrational states in a linear molecule with more than one bending mode, like DC_3N, are also labelled with the value of the total vibrational quantum number l_t, the sum of the individual l_i values, associated to each bending mode *i*. The vibrational states where only stretching modes are excited are classified always as Σ type, while for the case of bending excited states the following definitions apply:

$$\Sigma \rightarrow (l_t) = 0$$

$$\Pi \rightarrow (l_t) = 1$$
$$\Delta \rightarrow (l_t) = 2$$

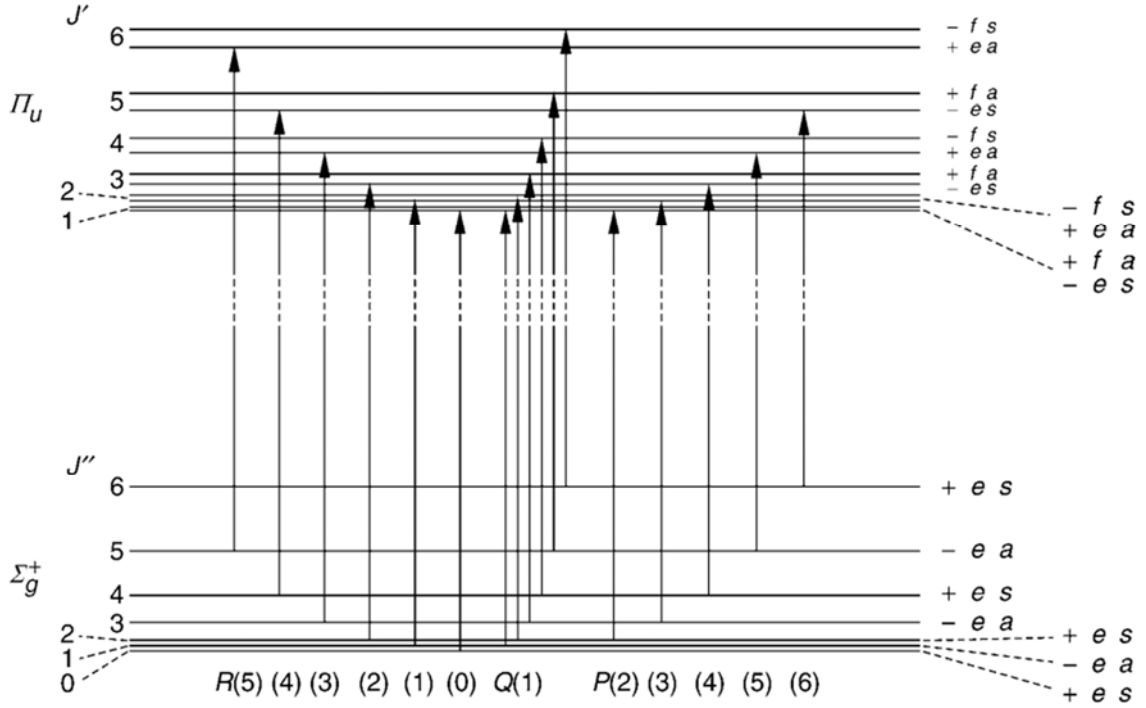

Figure 3.3. Rotational transitions accompanying a Π-Σ infrared vibrational transition in a linear polyatomic molecule with a centre of symmetry. For molecules without a centre of symmetry, the g and u subscripts and s and a label should be dropped [45].

In Figure 3.3 an example of Σ and Π states, with relative rotational splittings, is displayed. The rotational energy levels require additional labels to define the behaviour of the wavefunctions with respect to their parity, namely the inversion of the laboratory fixed coordinates of all atoms, identified by the ± signs. When the J dependence is factored out the *e/f* letters are used. As shown in Figure 3.3, Π states do not have an energy level with J=0, because J ≥ *l* and *l* =1.
The rotational selection rules are $e \leftrightarrow f$ for ΔJ = 0 (Q branch) and $e \leftrightarrow e, f \leftrightarrow f$ for ΔJ = ±1 (P and R branches). The vibrational selection rules are:

1) $\Delta l = 0$ with $l = 0$. This is parallel transition of the $\Sigma^+ - \Sigma^+$ type with P and R branches.
2) $\Delta l = \pm 1$. This is transition such as Π - Σ, Δ- Π and so forth with P and R branches and a strong Q branch.
3) $\Delta l = 0$ and $l \neq 0$. These transitions of type Π – Π, Δ – Δ, … with P and R branches and weak Q branches. [16].

3.4 Ro-vibrational Hamiltonian for DC_3N

After the previous description of the theoretical background for a linear molecule, I will now detail the specific Hamiltonian and the matrix elements for DC_3N, on which the analysis described in the following chapter is based.

Deuterated cyanoacetylene, a linear molecule with structure D ─ C ≡ C ─ C ≡ N, belongs to the $C_{\infty h}$ symmetry group. It has 7 vibrational modes: four stretching, of A symmetry, and three doubly degenerated bending modes, of E symmetry. The fundamental vibrational modes of DC_3N are listed in Table 3.1.

Table 3.1. Fundamental vibrational modes of DC_3N.

Modes	Description	ν_0 [cm^{-1}]	Reference
ν_1	C ─D stretching	2608.520	32
ν_2	C ≡ C stretching	2252.155	32
ν_3	C ≡ N stretching	1968.329	32
ν_4	C ─ C stretching	867.60	our global fit
ν_5	CCD bending	522.263933	our global fit
ν_6	CCC bending	492.759896	our global fit
ν_7	CCN bending	211.550293	our global fit

The ro-vibrational wave functions are represented as follows:

$$\Psi = \left|\nu_1, \nu_2, \nu_3, \nu_4, \nu_5^{l_5}, \nu_6^{l_6}, \nu_7^{l_7}, J, k\right\rangle_{e/f} \tag{27}$$

where l_t is a quantum number label the vibrational angular momentum associated to each bending mode and the *e/f* subscripts indicate the parity of the symmetrized wave functions described previously. The vibrational part of the wavefunction is expressed as a product of one- or two-dimensional harmonic oscillators. The rotational part is the symmetric-top wave-function with angular quantum number k given by $k = l_5 + l_6 + l_7$. Their form is given by the Wang-type linear combinations [46]:

$$\left|\nu_1,\nu_2,\nu_3,\nu_4,\nu_5^{l_5},\nu_6^{l_6},\nu_7^{l_7},J,k\right\rangle_{e/f} =$$
$$= \frac{1}{\sqrt{2}}\left|\nu_1,\nu_2,\nu_3,\nu_4,\nu_5^{l_5},\nu_6^{l_6},\nu_7^{l_7},J,k\right\rangle \pm (-1)^k \left|\nu_1,\nu_2,\nu_3,\nu_4,\nu_5^{-l_5},\nu_6^{-l_6},\nu_7^{-l_7},J,-k\right\rangle$$

(28)

$$\left|\nu_1,\nu_2,\nu_3,\nu_4,0^0,\ 0^0,\ 0^0,J,0\right\rangle_e = \left|\nu_1,\nu_2,\nu_3,\nu_4,0^0,\ 0^0,\ 0^0,J,0\right\rangle \qquad (29)$$

The upper and lower signs (±) correspond to *e* and *f* wave-functions, respectively. For Σ states (k = 0), the first non-zero l_t is chosen positive.

The effective Hamiltonian is made of three terms:

$$\hat{H} = \hat{H}_{vibrot} + \hat{H}_{l-type} + \hat{H}_{res} \qquad (30)$$

where

$\hat{H}_{vibrot}$ is the ro-vibrational energy including centrifugal distortion corrections. The parameters that will be determined (see Chapter 4) are the pure vibrational energy G_0, the *l*-dependent parameters x_L, y_L and r_{ab} and r_{abJ} constants, the rotational and centrifugal distortion constants B_v, D_v, H_v, L_v and their *l*-dependence d_{JL}.

$\hat{H}_{l-type}$ represents the *l*-type interaction between the *l* sub-levels of excited bending states. It included the q, q_J and q_{JJ} constants.

$\hat{H}_{res}$ accounts for resonances among accidentally quasi-degenerate ro-vibrational states. The part relative to the resonance Hamiltonian will not be detailed here, as it involves vibrational states not included in this thesis. It is however included in the global fit, which is relative to all the transitions detected for DC_3N. In Appendix the resonance constants are $C_{30}(466)$, $C_{30}(456)$, $C_{50}(47777)$, $C_{50J}(47777)$. The matrix elements of the effective Hamiltonian are expressed using the formalism already employed for the analysis of HC_3N [33]. The reader is reminded to equations 4-8 of Ref. [33].

4. ANALYSIS OF THE SPECTRA

Literature data were available for some of analyzed states as described in the introduction and were used as initial constants to predict the positions of the ro-vibrational transitions. The prediction of the band centers was based on references [26, 29]. The preliminary investigation was conducted using Pickett's SPCAT and home-made programs. Every experimental band was analysed using Wspectra and Pgopher programs. Pickett's SPFIT program was used for fitting the data [47, 48].

Table 4.1. List of bands of DC_3N analysed in this work.

Transitions observed and analysed
$\nu_1 \leftarrow$ GS
$\nu_2 \leftarrow$ GS
$\nu_3 \leftarrow$ GS
$\nu_7 \leftarrow$ GS
$2\nu_7 \leftarrow \nu_7$
$\nu_5 \leftarrow \nu_7$
$\nu_5+\nu_7 \leftarrow 2\nu_7$
$\nu_6+\nu_7 \leftarrow 2\nu_7$
$4\nu_7 \leftarrow 2\nu_7$

4.1 Assignment and analysis of the FIR region

The experimental spectrum recorded at SOLEIL was limited to the FIR region. In the low energy range (150 cm^{-1} – 450 cm^{-1}) six fundamental, overtone, combination and hot bands involving the bending modes were analysed: $\nu_7 \leftarrow$ GS, $2\nu_7 \leftarrow \nu_7$, $\nu_5 \leftarrow \nu_7$, $\nu_5+\nu_7 \leftarrow 2\nu_7$, $\nu_6+\nu_7$

← $2\nu_7$, $4\nu_7$ ← $2\nu_7$. Figure 4.1 shows the recorded spectrum with the analysed bands. The spectra contain transitions due to CO, H_2O and HC_3N. Therefore, during the analysis, HC_3N spectra recorded in the same range and literature data for CO, H_2O were used to recognize and eliminate the interfering lines. Figure 4.2 presents two spectra (DC_3N and HC_3N) in the 190 – 230 cm^{-1} wavenumber region, where the fundamental band ν_7 ← GS and the hot band $2\nu_7$ ← ν_7 of DC_3N have their origin.

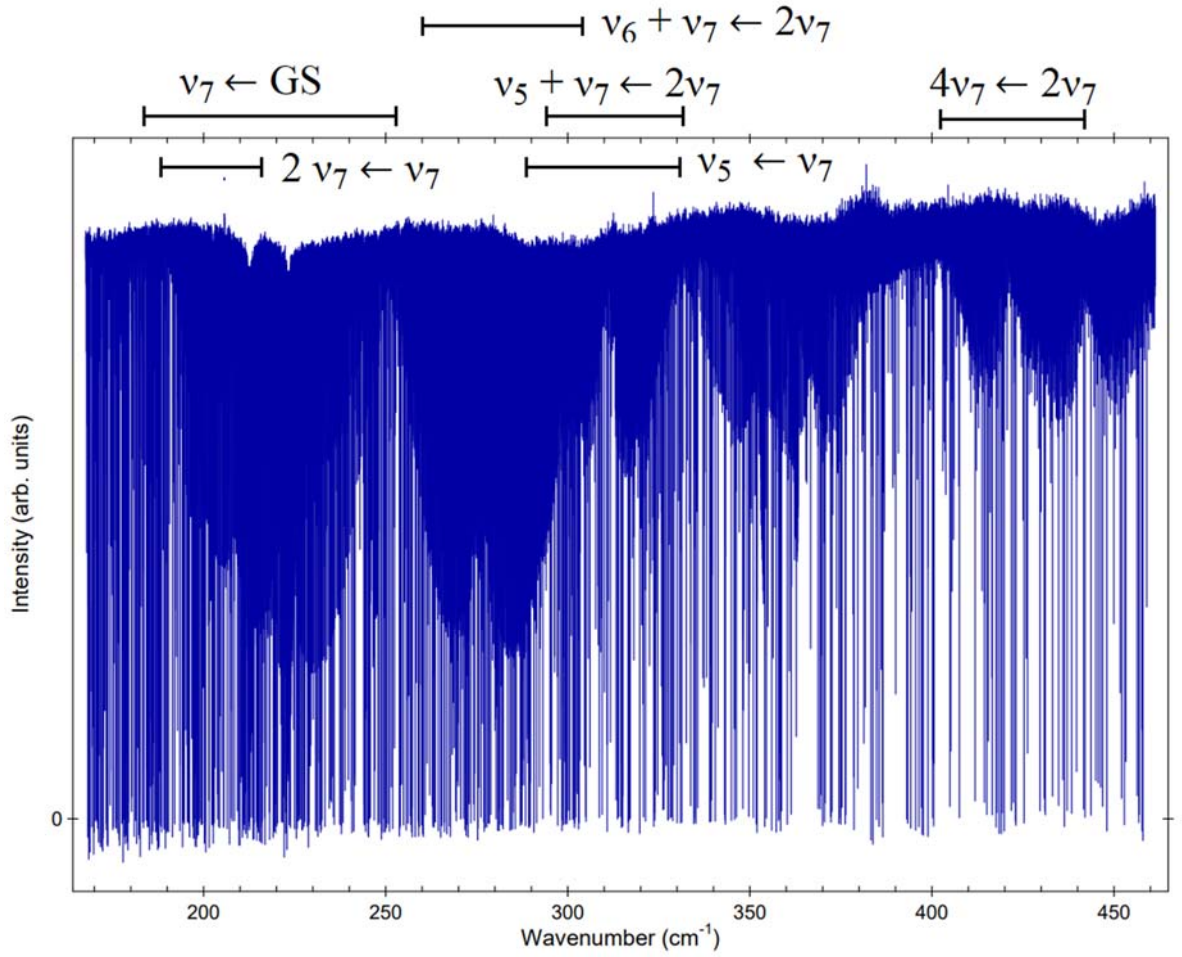

Figure 4.1. Experimental spectra of DC_3N recorded at SOLEIL synchrotron in the range 170 – 460 cm^{-1} with the bands analysed in this work.

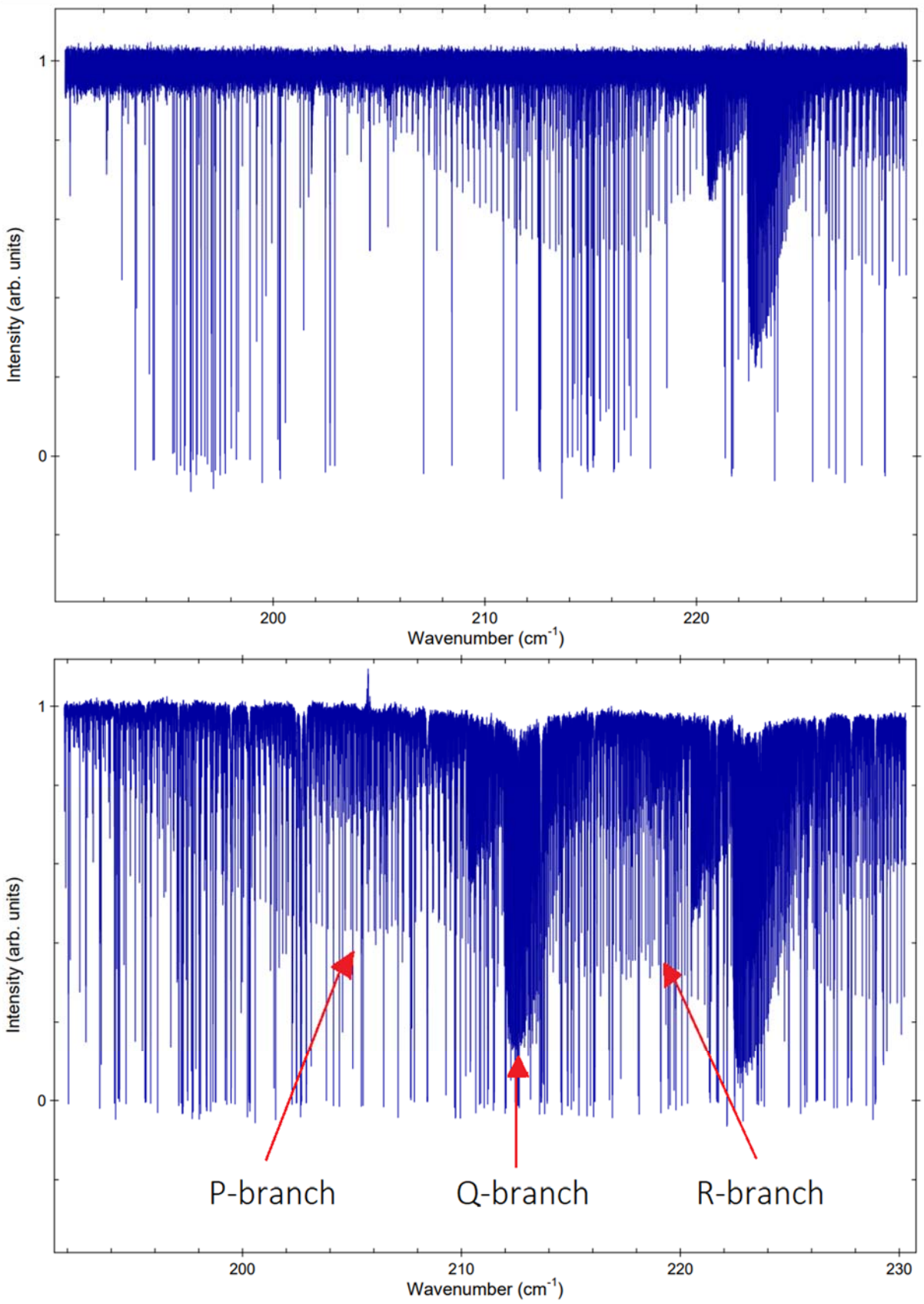

Figure 4.2. FIR spectrum of HC_3N (upper trace) and DC_3N (lower trace) in the range 190 – 230 cm^{-1} recorded at SOLEIL. The P, Q and R branches of the $\nu_7 \leftarrow$GS fundamental band are highlighted.

4.2 The ν_7 fundamental and the $2\nu_7 \leftarrow \nu_7$ hot bands

One of vibrational modes of DC_3N is the CCN bending mode, called ν_7, whose fundamental vibrational transition is centered at 212.06 cm^{-1} [29]. In this work, many transitions were assigned from the recorded spectra for P, Q and R-branches. In this region, the hot band $2\nu_7 \leftarrow \nu_7$ has been analyzed as well. Since the $\nu_7 = 2$ state is formed of two sub-states of symmetry Σ^+ and Δ and $\nu_7 = 1$ is a Π state, the possible subbands allowed for this transition are $\Sigma^+ - \Pi$ and $\Delta - \Pi$. Due to the high resolution of the recorded spectra, transitions that belong to these bands were observed with no misassignments. Eventually, 258 lines (in the energy range 184 – 246 cm^{-1} and J = 1 – 90) were assigned for $\nu_7 \leftarrow$ GS and 191 (J = 2 – 85) lines were assigned to the $2\nu_7 \leftarrow \nu_7$ subbands.

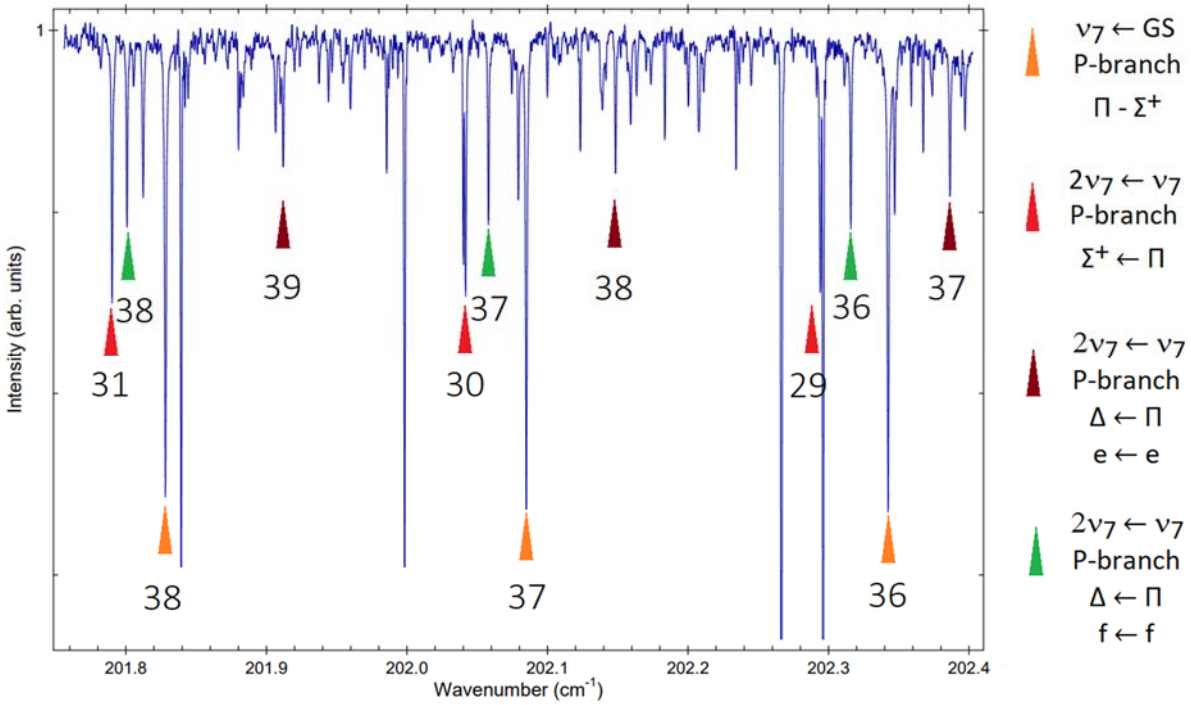

Figure 4.3. DC_3N spectrum (in the 201.75 – 202.4 cm^{-1} range) with assigned transitions that belong to the $\nu_7 \leftarrow$ GS band (orange), $2\nu_7 \leftarrow \nu_7$ subbands (red, brown, green) described in the legend. Numbers below the marks represent the value of J upper for every transition.

Figure 4.3 presents a detail of the DC_3N spectrum (in the 201.75 – 202.4 cm^{-1} range) with some assigned transitions belonging to $\nu_7 \leftarrow$ GS and $2\nu_7 \leftarrow \nu_7$. It is important to point out that high resolution was essential to measure the line wavenumbers with high precision, because the

density of lines is often very high. In Table 4.2, the transition wavenumbers (cm^{-1}) and the corresponding J quantum numbers of Fig. 4.3 are listed.

Table 4.2. List of assigned transitions of $\nu_7 \leftarrow$ GS band and $2\nu_7 \leftarrow \nu_7$ subbands of DC_3N in the energy range 201.75 – 202.4 cm^{-1} showed in Fig. 4.3.

Band	J	Position (cm^{-1})
$\nu_7 \leftarrow$ GS $\Pi - \Sigma^+$ P-branch	36	202.3424732
	37	202.0849522
	38	201.8281083
$2\nu_7 \leftarrow \nu_7$ $\Sigma^+ - \Pi$ P-branch	29	202.2942300
	30	202.0417076
	31	201.7901460
$2\nu_7 \leftarrow \nu_7$ $\Delta - \Pi$ P-branch e←e	37	202.3865305
	38	202.1485406
	39	201.9119597
$2\nu_7 \leftarrow \nu_7$ $\Delta - \Pi$ P-branch f←f	36	202.3159610
	37	202.0580235
	38	201.8007098

4.3 The $\nu_5 \leftarrow \nu_7$ and $\nu_5+\nu_7 \leftarrow 2\nu_7$ bands

The ν_5 vibrational mode of DC_3N is associated to the CCD bending motion and its fundamental transition can be found around 500 cm^{-1}, therefore outside the studied range. However, the transitions $\nu_5 \leftarrow \nu_7$ is located between 280 and 330 cm^{-1}, in the FIR region investigated. The symmetry of both states is Π. As far as the P and R branches are concerned, two types of transitions can be observed according to the parity selection rules *e* – *e* and *f* – *f*. 268 lines have been assigned.

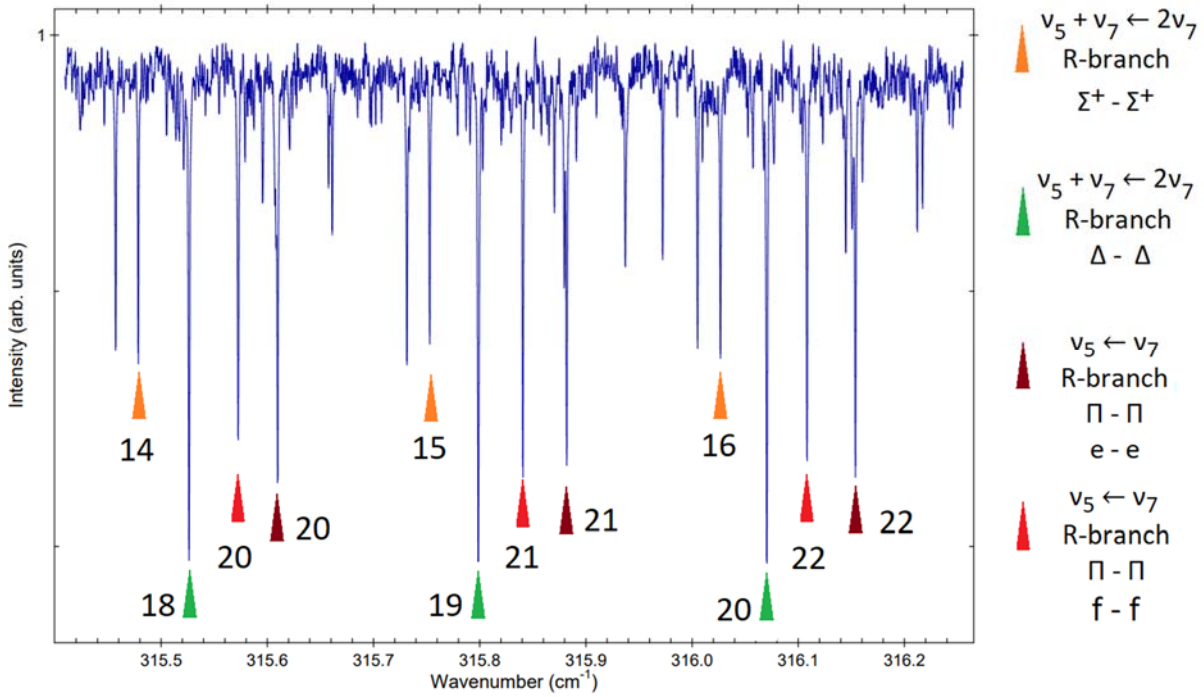

Figure 4.4. DC_3N spectrum (in the 315.40 – 316.24 cm^{-1} range) with assigned transitions that belong to $\nu_5 \leftarrow \nu_7$ (red and brown) and $\nu_5+\nu_7 \leftarrow 2\nu_7$ subbands (orange, green) described in the legend on the right. Numbers below marks represent the value of J upper for every transition.

In the same region of the spectrum one more band was investigated. A set of 278 transitions was assigned to the $\nu_5+\nu_7 \leftarrow 2\nu_7$ combination band. For both states involved in the transition, Σ^+ and Δ substates arise. Possible transitions coming from $\Sigma^+ - \Sigma^+$ and $\Delta - \Delta$ subbands were thoroughly investigated. In this case, $e - e$ and $f - f$ transitions were overlapped and appeared as one spectral line with higher intensity. This is presented in Figure 4.4, where green marks correspond to $\Delta - \Delta$ overlapped transitions. In the same figure, some transitions belonging to $\Sigma^+ - \Sigma^+$ subbands (orange) are also showed along with $\Delta - \Delta$ for $e - e$ (brown) and $f - f$ (red). Table 4.3 summarize the transitions assigned for this bands in the portion 315.40 – 316.24 cm^{-1} of the spectrum.

Table 4.3. List of assinged transitions of $\nu_5 \leftarrow \nu_7$ and $\nu_5+\nu_7 \leftarrow 2\nu_7$ subbands of DC_3N in the energy range 315.40 – 316.24 cm^{-1} showed in Fig 4.4.

Band	J	Position (cm^{-1})
$\nu_5 + \nu_7 \leftarrow 2\nu_7$ $\Sigma^+ - \Sigma^+$ R-branch	14	315.4784551
	15	315.7529291
	16	316.0268138
$\nu_5 + \nu_7 \leftarrow 2\nu_7$ $\Delta - \Delta$ R-branch	18	315.5262475
	19	315.7987004
	20	316.0704686
$\nu_5 \leftarrow \nu_7$ $\Pi - \Pi$ R-branch e - e	20	315.6096871
	21	315.8820029
	22	316.1538677
$\nu_5 \leftarrow \nu_7$ $\Pi - \Pi$ R-branch f - f	20	315.5725423
	21	315.8407377
	22	316.1083282

4.4. $\nu_6+\nu_7 \leftarrow 2\nu_7$ combination band and $4\nu_7 \leftarrow 2\nu_7$ hot band

In this thesis two more bands were investigated in the FIR region, 440 transitions belonging to the $\nu_6+\nu_7 \leftarrow 2\nu_7$ band were assigned in the 261 – 305 cm^{-1} energy range and 349 transitions of the $4\nu_7 \leftarrow 2\nu_7$ band from 403 to 440 cm^{-1}. The theoretical description of the transition for these two bands are analogous to the ones of $\nu_5+\nu_7 \leftarrow 2\nu_7$ described above.

4.5. Summary of the FIR region assignments

During the analysis of the FIR spectrum of DC_3N, 1784 transition were assigned to six fundamental, combination and hot bands. They are summarized in Table 4.4 where the wavenumber range, J values and number of data used in the analysis are reported. An energy-level diagram of DC_3N up to 1015 cm^{-1} is shown in Figure 4.5. In this figure, only the investigated states are presented, the arrows representing the FIR bands analyzed in this work. The full list of transitions added to global analysis of DC_3N spectrum is available from the authors of this work.

Table 4.4. Ro-vibrational bands analyzed in the FIR region for DC_3N.

Band	Notation	Sub-bands	Wavenumber range (cm^{-1})	J range	Number of lines
$\nu_7 \leftarrow$ GS	(0001)←(0000)	Π - Σ^+	184 - 246	1 – 90	258
$2\nu_7 \leftarrow \nu_7$	(0002)←(0001)	(Σ^+ , Δ)- Π	188 - 210	2 – 85	191
$\nu_5 \leftarrow \nu_7$	(0100)←(0001)	Π - Π	287- 331	1 – 80	268
$\nu_5+\nu_7 \leftarrow 2\nu_7$	(0101)←(0002)	(Σ^+, Δ) - (Σ^+, Δ)	292 - 330	2 – 84	278
$\nu_6+\nu_7 \leftarrow 2\nu_7$	(0011)←(0002)	(Σ^+, Δ) - (Σ^+, Δ)	261 - 305	3 – 84	440
$4\nu_7 \leftarrow 2\nu_7$	(0004)←(0002)	(Σ^+, Δ) - (Σ^+, Δ)	403 - 440	2 – 70	349

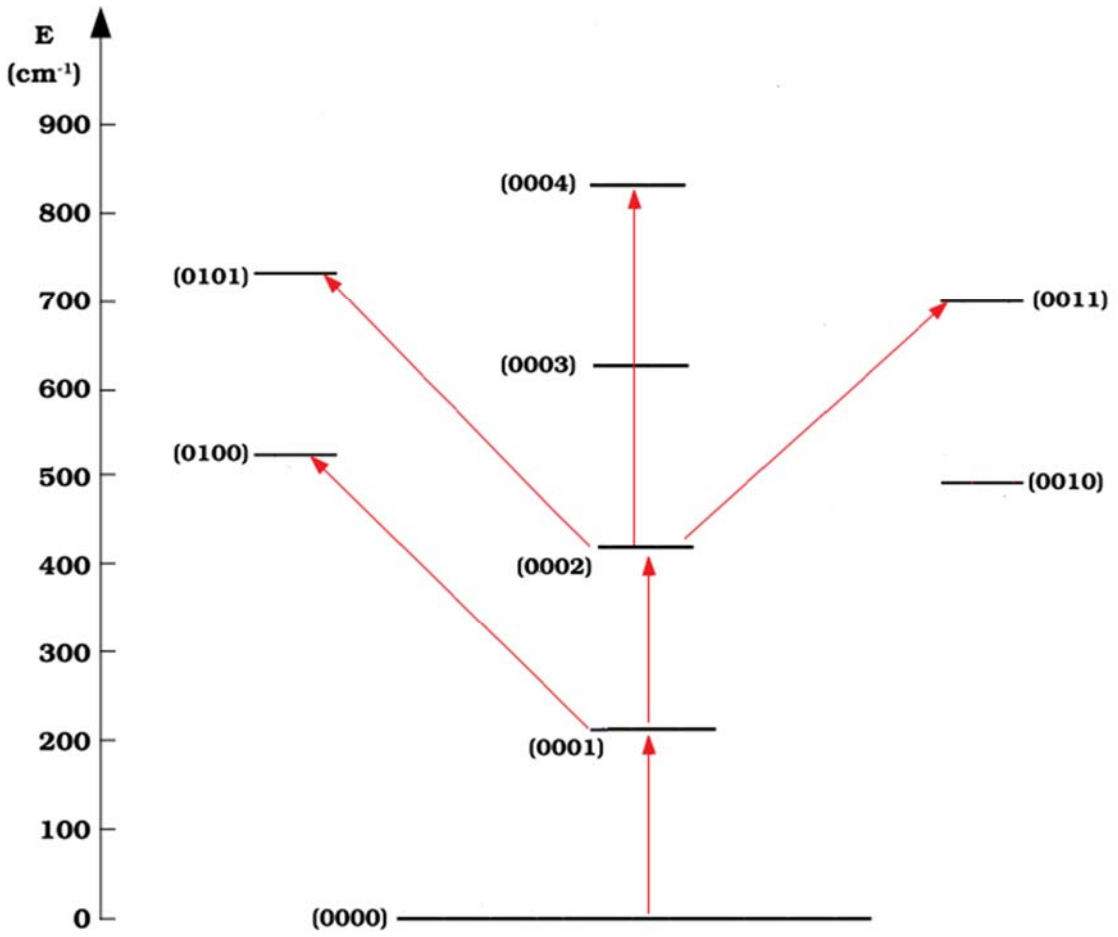

Figure 4.5. Vibrational energy-level diagram of the states investigated in this work in FIR region for DC_3N. The arrows represent the 6 analyzed bands described in detail in Table 4.4.

4.6 Vibrational stretching modes region

It requires more energy to stretch (or compress) a bond than to bend it, and as it might be expected, the energy or frequency that characterizes the stretching vibration is higher than for bending modes. In the second part of my project I investigated the three fundamental stretching modes of deuterated cyanoacetylene spectra in the range 1900 – 2800 cm^{-1}. These spectra were recorded using the Bomem Fourier Transform Spectrometer in Bologna at the maximum resolution achievable (0.004 cm^{-1}). The first three fundamental stretching modes of DC_3N, ν_1, ν_2, ν_3 correspond to the C-D, C≡C and C≡N bond stretching, respectively. After a preliminary investigation using the parameters from a low resolution study [26], the band origin positions

(ν_0) were calculated (See Table 4.5) and a number of transitions were assigned. For these fundamental transitions, only $\Sigma^+ - \Sigma^+$ bands are allowed and the P and R branches were assigned easily. They are listed in Table 4.6 with the corresponding J and wavenumber ranges. Two different pressures were employed, in order to detect also weak transitions (16 and 32 Pa). For the strong ν_1 and ν_3 fundamental bands, the transitions were assigned from the lower pressure spectrum, where the lines are not saturated. The corresponding spectroscopic constants were derived from a fitting program and were very close to the constants already reported in previous work [32]. The total number of assigned transitions for the first three stretching modes is 515. A full list of transitions is available from the authors of this work.

Table 4.5. Band center position for first three stretching modes of DC_3N.

Modes	ν_0 [cm^{-1}]
$\nu_1 \leftarrow$ GS	2608.5178
$\nu_2 \leftarrow$ GS	2252.1390
$\nu_3 \leftarrow$ GS	1968.3288

Table 4.6. Ro-vibrational bands analyzed in the 1900 – 2800 cm^{-1} wavenumber region of DC_3N.

Band	Wavenumber range (cm^{-1})	J range	Number of lines
$\nu_1 \leftarrow$ GS	2582 - 2631	5 – 92	164
$\nu_2 \leftarrow$ GS	2219 - 2271	3 – 97	173
$\nu_3 \leftarrow$ GS	1940 - 1991	5 – 96	178

4.7 Global fit and derived spectroscopic constants

In total, 2299 transitions belonging to 9 fundamental, overtone, combination and hot bands have been assigned in two wavenumber ranges for DC_3N. They are three of the fundamental stretching bands (ν_1, ν_2, ν_3) and 6 bands involving the bending modes ν_5, ν_6 and ν_7 ($\nu_7 \leftarrow$ GS, $2\nu_7 \leftarrow \nu_7$, $\nu_5 \leftarrow \nu_7$, $\nu_5+\nu_7 \leftarrow 2\nu_7$, $\nu_6+\nu_7 \leftarrow 2\nu_7$, $4\nu_7 \leftarrow 2\nu_7$). The obtained data set was analysed in a weighted global-fit procedure which included also previous bands assigned for this molecule. The fit consists of 30 infrared bands and 7145 transitions exploring all vibrational modes of DC_3N and including both pure rotational and ro-vibrational data. The data were fitted to the Hamiltonian presented in Chapter 3 and its coefficients optimized in an iterative least-squares procedure. The results of the global fit are in Appendix, where the list of the obtained spectroscopic constants is reported band by band. The number of bands, their RMS error as calculated in the fit and the overall weighted RMS error are also reported. It can be appreciated that the quality of the fit is very high and the parameters calculated with high precision.

As far as the data of this project are concerned, uncertainties between 0.0004 and 0.00075 cm^{-1} were used for the measurements performed in Bologna and between 0.00005 and 0.0001 cm^{-1} for transitions recorded in the FIR region. The spectroscopic parameters obtained from the global fit procedure for the bands analysed in this thesis are in Tables in Tables 4.7 – 4.10. As anticipated, the analysis of DC_3N follows the approach successfully adopted for HC_3N [33] and many experimental data of investigated states are now available.

Table 4.7. Spectroscopic constants derived for DC_3N in the ground state and singly-excited stretching states. Numbers in parenthesis are one standard deviation in units of the last quoted digit.

Constant	Unit	Ground state	$\nu_1 = 1$	$\nu_2 = 1$	$\nu_3 = 1$
G_v	cm^{-1}	0.0	2608.518327(58)	2252.138828(59)	1968.328179(58)
B_v	MHz	4221.580853(36)	4210.2179(18)	4203.7900(20)	4209.9044(17)
D_v	kHz	0.4517857(89)	0.44988(41)	0.45509(49)	0.45297(37)
H_v	mHz	0.03949(77)	0.139(26)	0.366(32)	0.096(22)
L_v	nHz	- 0.153(22)	-0.153	-0.153	-0.153

Table 4.8. Spectroscopic constants derived for DC_3N in the singly-excited bending states. Numbers in parenthesis are one standard deviation in units of the last quoted digit.

Constant	Unit	$\nu_5 = 1$	$\nu_7 = 1$
G_v	cm^{-1}	522.2639330(49)	211.5502859(33)
B_v	MHz	4225.835835(71)	4234.519465(31)
D_v	kHz	0.452490(14)	0.4718865(59)
H_v	mHz	0.03949	0.08240(30)
L_v	nHz	-0.153	-0.153
q_t	MHz	2.68903(13)	5.907823(55)
q_{tJ}	Hz	-1.627(27)	-13.646(11)
q_{tJJ}	μHz	-	43.37(57)

Table 4.9. Spectroscopic constants derived for DC_3N in the combination states. Numbers in parenthesis are one standard deviation in units of the last quoted digit.

Constant	Unit	$\nu_7 = \nu_5 = 1$	$\nu_7 = \nu_6 = 1$
G_v	cm^{-1}	734.058721(13)	703.8550157(94)
$x_{L(aa)}$	GHz	-	56.39
$x_{L(bb)}$	GHz	19.5125	19.3189
$x_{L(ab)}$	GHz	23.13131(38)	16.16651(21)
r_{ab}	GHz	0.32219(69)	-17.04625(41)
r_{abJ}	kHz	-65.965(71)	-5.784(70)
B_v	MHz	4238.741823(94)	4242.274182(82)
D_v	kHz	0.472594(28)	0.481887(24)
H_v	mHz	0.03949	0.03949
L_v	nHz	-0.153	-0.153
$d_{JL(aa)}$	kHz	-	-11.254
$d_{JL(bb)}$	kHz	-9.971	141.5
$d_{JL(ab)}$	kHz	-5.08(13)	43.88(12)
q_a	MHz	2.70634(31)	3.17827(15)
q_{aJ}	Hz	-1.626	-1.571
q_b	MHz	5.90943(72)	5.94427(18)
q_{aJ}	Hz	-13.738(97)	-13.646
q_{bJJ}	μHz	43.37	43.37

Table 4.10. Spectroscopic constants derived for DC_3N in overtone states. Numbers in parenthesis are one standard deviation in units of the last quoted digit.

Constant	Unit	$\nu_7 = 2$	$\nu_7 = 4$
G_v	cm^{-1}	422.3753581(60)	841.9860892(94)
$x_{L(tt)}$	GHz	19.354043(61)	19.03874(51)
$y_{L(tt)}$	MHz	-	1.82(12)
B_v	MHz	4247.45224(11)	4273.30576(21)
D_v	kHz	0.491827(21)	0.53448(11)
H_v	mHz	0.03949	0.176(21)
L_v	nHz	-0.153	-0.153
$d_{JL(tt)}$	kHz	-10.426(30)	-11.368(21)
$h_{JL(tt)}$	Hz	-	-0.0552(63)
q_t	MHz	5.93258(10)	5.98281(15)
qt_J	Hz	-13.897	-14.288(46)
q_{tJJ}	µHz	43.37	43.37

5. CONCLUSIONS

The aim of this project it the study and deuterated cyanoacetylene DC_3N by high-resolution molecular spectroscopy. Cyanoacetylene and its deuterated form are molecules of great astronomical importance. For example, HC_3N is a potential tracer of the evolution of star forming regions. It has been observed in number of sources both Galactic and extragalactic and these detections relied on previous laboratory investigations. On the other hand, DC_3N is less studied than the main isotopologue and experimental data lack some essential information concerning its infrared spectrum.

In this thesis, a large set of high-resolution ro-vibrational data of deuterated cyanoacetylene has been investigated. This analysis included Fourier transform infrared spectra of DC_3N recorded at SOLEIL synchrotron and in Bologna in two energy regions: 150 – 450 cm^{-1} and 1800 – 2800 cm^{-1} respectively. This work allowed to obtain very precise experimental data for both vibrational transitions already studied in the past and for those which have never been detected before. Nine fundamental, overtone, combination and hot bands have been analysed: ν_1, ν_2, ν_3, ν_7, $2\nu_7 \leftarrow \nu_7$, $4\nu_7 \leftarrow 2\nu_7$, $\nu_5 \leftarrow \nu_7$, $\nu_5+\nu_7 \leftarrow 2\nu_7$, $\nu_6+\nu_7 \rightarrow 2\nu_7$. A total of 2299 transitions have been assigned. These data, together with the bands previously studied for DC_3N were analysed in a global fit which yielded a large number of very precise spectroscopic parameters, which included rotational, vibrational and resonance constants.

This work improves considerably the previous spectroscopic knowledge of DC_3N, which was limited to low resolution studies [26, 27, 31]. Not all the bands that have been observed in our FIR and IR experiments have been analysed so far. Therefore, further research and detailed analysis of DC_3N spectrum in the recorded regions can be performed. We plan also to extend the infrared region observed to higher energies, in order to detect the stretching overtone bands. The data recorded for deuterated cyanoacetylene can be very useful to assist future astronomical observations of this species.

6. REFERENCES

[1] S. Yamamoto, Introduction to Astrochemistry, Astronomy and Astrophysics Library 7, 2017.

[2] Anil K. Pradhan, Sultana N. Nahar, Atomic Astrophysics and Spectroscopy, Cambridge University Press, 2011.

[3] A. McKellar, Evidence for the molecular origin of some hithero unidetified interstellar lines, Publications of the Astronomical Society of the Pacific, 52, 307, 1940.

[4] K. M. Merrill, S. T. Ridgway, Infrared spectroscopy of stars, Annual Review Astronomy and Astrophysics, 17, 9-4, 1979.

[5] John H. Black, The High-Resolution Frontier in Infrared Spectroscopy, High Resolution Infrared Spectroscopy in Astronomy, 3–14, 2005.

[6] D. E. Jennings, F. M. Flasar, V. G. Kunde, A. Nixon, M. E. Segura, P. N. Romani, N. Gorius, S. Albright, J. C. Brasunas, R. C. Carlson, A. A. Mamoutkine, E. Guandique, M. S. Kaelberer, S. Aslam, R. K. Achterberg, G. L. Bjoraker, C. M. Anderson, V. Cottini, J. C. Pearl, M. D. Smith, B. E. Hesman, R. D. Barney, S. Calcutt, T. J. Vellacott, L. J. Spilker, S. G. Edington, S. M. Brooks, P. Ade, P. J. Schinder, A. Coustenis, R. Ccourtin, G. Michael, R. Fettig, S. Pilorz, C. Ferrari, The Composite Infrared Spectrometer (CIRS) on Cassini, Applied Optics, 56, 18, 5274-5294, 2017.

[7] James Webb Space Telescope, NASA, https://jwst.nasa.gov.

[8] B. A. McGuire, Census of Interstellar, Circumstellar, Extragalactic, Protoplanetary Disk, and Exoplanetary Molecules, The Astrophysical Journal Supplement Series, 239, 2, 48, 2018.

[9] E. van Dishoeck, G. A Blake, Chemical evolution of star-forming regions, Annual Review Astronomy and Astrophysics, 317-368, 36, 1998.

[10] Loomis, R.A., Burkhardt, A.M., Charnley, S.B., Cordiner, M.A., Herbst, E., Kalenskii, S., Lee, K.L.K., McCarthy, M.C., Remijan, A.J., Shingledecker, C.N., Willis, E.R., Xue, C. McGuire,, A rigorous investigation of spectral line stacking and matched filter techniques: Application to the dection of $HC_{11}N$, Nature Astronomy, *in revision*, 2020.

[11] J.-C. Loison, V. Wakelam, K. M. Hickson, A. Bergeat, R. Mereau, The gas-phase chemistry of carbon chains in dark cloud chemical models, Monthly Notices of the Royal Astronomical Society 437, 930–945, 2014.

[12] E. Herbst, E. F. van Dishoeck, Complex organic interstellar molecules, Annual Review of Astronomy and Astrophysics, 47, 427–480, 2009.

[13] A. Belloche, H. S. P. Müller, R. T. Garrod, and K. M. Menten, Exploring molecular complexity with ALMA (EMoCA): Deuterated complex organic molecules in Sagittarius

B2(N2), Astronomy & Astrophysics 587, A91, 2016.
[14] V.M. Rivilla, M. N. Drozdovskaya, K. Altwegg, P. Caselli, M. T. Beltran, F. Fontani, F. F. S. van der Tak, R. Cesaroni, A. Vasyunin, M. Rubin, F. Lique, S. Marinakis, L. Testi, Monthly Notices of the Royal Astronomical Society, 492, 1-20, 2020.
[15] R. L. DeLeon, J. S. Muenter, Molecular beam electric resonance study of the ground and excited states of cyanoacetylene, The Journal of Chemical Physics, 82, 1702, 1985.
[16] G. Winnewiser, C. M. Walmsley, Carbon chain molecules in interstellar clouds, Astrophysics and Space Science, 65, 83-93, 1979.
[17] A. Jolly, Y. Benilan, A. Fayt, New infrared integrated band intensities for HC_3N and extensive line list for the ν_5 and ν_6 bending modes, Journal of Molecular Spectroscopy, 242, 46-54, 2007.
[18] W. Langer, F. Schloerb, R. Snell, J. Young, Detection of deuterated cyanoacetylene in the interstellar cloud TMC-1, The Astrophysical Journal, 239, 125-128, 1980.
[19] A. J. Al-Edhari, C. Ceccarelli, C. Kahane, S. Viti, N. Balucani, E. Caux, A. Faure, B. Lefloch, F. Lique, E. Mendoza, D. Quenard, L. Wiesenfeld, History of the solar-type protostar IRAS 16293–2422 as told by the cyanopolyynes, Astronomy & Astrophysics 597, A40, 2017.
[20] N. Sakai, T. Sakai, T. Hirota, S. Yamamoto, Deuterated molecules in warm carbon chain chemistry: The L1527 case, The Astrophysical Journal, 702, 1025 – 1035, 2009.
[21] M. A. Cordiner, C. A. Nixon, N.A. Teanby, P. G. J. Irwin, J. Sergiano, S. B. Charnlry, S. N. Milam, M. J. Mumma, D. C. Lis, G. Villanueva, L. Paganini, Y.-J. Kuan, A. J. Remijan, ALMA measurements of the HNC and HC_3N distributions in titan's atmosphere, The Astrophysical Journal Letters, 795, L30, 2014.
[22] E. Bianchi, C. Codella, C. Ceccarelli, F. Vazart, R. Bachiller, N. Balucani, M. Bouvier, M. De Simone, J. Enrique-Romero, C. Kahane, B. Lefloch, A. López-Sepulcre, J. Ospina-Zamudio, L. Podio, V. Taquet, The census of interstellar complex organic molecules in the Class I hot corino of SVS13-A, Monthly Notices of the Royal Astronomical Society, 483, 2, 2019.
[23] G. B. Esplugues, J. Cernicharo, S. Viti, J. R. Goicoechea, B. Tercero, N. Marcelino, A. Palau, T. A. Bell, E. A. Bergin, N. R. Crockett, S. Wang, Combined IRAM and Herschel/HIFI study of cyano(di)acetylene in Orion KL: tentative detection of DC_3N, Astronomy & Astrophysics, 559, A51, 2013.
[24] A. Belloche, H. Muller, R. Garrod, K. Menten, Exploring molecular complexity with ALMA (EMoCA): Deuterated complex organic molecules in Sagittarius B2 (N2), Astronomy & Astrophysics, 587, A91, 2016.
[25] V. M. Rivilla, L. Colzi, F. Fontani, M. Melosso, P. Caselli, L. Bizzocchi, F. Tamassia, L.

Dore. DC_3N towards a sample of high-mass star-forming regions, Monthly Notices of the Royal Astronomical Society, 496, 1990, 2020.
[26] Y. Benilan, A. Jolly, F. Raulin, J.-C. Guillemin, IR band intensities of DC_3N and $HC_3{}^{15}N$: Implication for observations of Titan's atmosphere, Planetary and Space Science 54, 6, 2006.
[27] P. D. Mallison, R. L. de Zafra, The microwave spectrum of cyanoacetylene in ground and excited vibrational states, Molecular Physics, 36, 3, 1978.
[28] G. Plummer, D. Mauer, K. Yamada, K. Moller, Rotational spectra of DC_3N in some excited vibrational states, Journal Molecular Spectroscopy, 130, 2, 1988.
[29] H. Spahn, H. S. Muller, T. F. Giesen, J.-U. Grabow, M. E. Harding, J. Gauss, S. Schlemmer, Rotational spectra and hyperfine structure of isotopic species of deuterated cyanoacetylene, DC_3N, Chemical Physics 346, 1-3, 2008.
[30] M. Uyemura, S. Deguchi, Y. Nakada, T. Onaka, Infrared intensities of bending fundamentals in gaseous HCCCN and DCCCN, Chemical Society of Japan, 55, 2, 1982.
[31] B. Coveliers, W. Ahmed, A. Fayt, H. Burger, Far-infrared spectra of DCCCN, Journal of Molecular Spectroscopy 156, 1, 1992.
[32] P. Mallinson, A. Fayt, High resolution infra-red studies of HCCCN and DCCCN, Molecular Physics, 32, 2, 1976.
[33] L. Bizzocchi, F. Tamassia, J. Laa, B. M. Giuliano, C. Degli Esposti, L. Dore, M. Melosso, E. Canè, A. Pietropolli Charmet, H. S. P. Müller, Rotational and high-resolution infrared spectrum of HC_3N: Global ro-vibrational analysis and improved line catalog for astrophysical observations, The Astrophysical Journal Supplement Series, 233, 11, 20, 2017.
[34] C. Moureu, J. C. Bongrand, Le cyanoacetylene C_3NH, Annales de Chimie, 14, 47-58, 1920.
[35] F.A. Miller, D.H. Lemmon, The infrared and Raman spectra of dicyanodiacetylene, Spectrochimica Acta Part A: Molecular Spectroscopy, 23A, 1415 – 1423, 1967.
[36] R. A. Toth, ν_2 band of $H_2{}^{16}O$: line strengths and transition frequencies. J. Opt. Soc. Am. B, 8, 2236, 1991.
[37] I. E. Gordon, L. S. Rothman, C. Hill, R. V. Kochanov, Y. Tan, P. F. Bernath, M. Birk, V. Boudon, A. Campargue, K. Chance, et al., The HITRAN2016 Molecular Spectroscopic Database, J. Quant. Spectrosc. Rad. Trans. 203, 3–69, 2017.
[38] J.-B. Brubach, L. Manceron, M. Rouzieres, O. Pirali, D. Balcon, F. Kwabia-Tchana, V. Boudon, M. Tudorie, T. Huet, 311 A. Cuisset, P. Roy, Performance of the AILES THz-Infrared beamline at SOLEIL for High resolution spectroscopy, WIRMS 2009, 1214 of AIP Conference Proceedings, 2010.
[39] O. Pirali, V. Boudon, J. Oomens, M. Vervloet, Rotationally resolved infrared spectroscopy

of adamantane, The Journal of Chemical Physics, 024310, 136, 2012.
[40] F. Matsushima, H. Odashima, T. Iwasaki, S. Tsunekawa, K. Takagi, Frequency-measurement of pure rotational transitions of H_2O from 0.5 to 5 THz, J. Mol. Struct. 352, 1995.
[41] V. M. Horneman, R. Anttila, S. Alanko, J. Pietila, Transferring calibration from CO_2 laser lines to far infrared water lines with the aid of the ν_2 band of OCS and the ν_2, ν_1- ν_2, and ν_1+ ν_2 bands of $^{13}CS_2$: Molecular constants of 13CS2 , J. Mol. Spectrosc. 234, 2, 2005.
[42] W. Gordy, R. L. Cook, Microwave molecular spectra, John Wiley & Sons, 1984.
[43] P. F. Bernath, Spectra of atoms and molecules, Oxford University Press, 1995.
[44] V. P. Solovjov, B. W. Webb, F. Andre, Radiative Properties of Gases, Handbook of Thermal Science and Engineering, 2017.
[45] J. M. Hollas, Modern Spectroscopy, John Wiley & Sons, 1987.
[46] K. M. T. Yamada, F. W. Birss, M.R. Aliev, Effective Hamiltonian for Polyatomic Linear Molecules, Journal of Molecular Spectroscopy 112, 347-356, 1985.
[47] http://pgopher.chm.bris.ac.uk/
[48] https://spec.jpl.nasa.gov/

APPENDIX

RESULTS OF THE GLOBAL FIT

For each vibrational state included in the analysis the associated spectroscopic parameters are given in the left column, their units in the middle column and their values in the right column. Numbers in parenthesis are one standard deviation in units of the last quoted digit. Numbers without error have been fixed in the analysis.

****

GS ground state

****

G_0		0.0
B_0	MHz	4221.580853(36)
D_0	kHz	0.4517857(89)
H_0	mHz	0.03949(77)
L_0	nHz	-0.153(22)

****

$v_7 = 1$

****

G_v	cm^{-1}	211.5502859(33)
x_{L77}	GHz	19.5125
B_v	MHz	4234.519465(31)
D_v	kHz	0.4718865(59)
H_v	mHz	0.08240(30)
L_v	nHz	-0.153
d_{JL77}	kHz	-9.971
q_7	MHz	5.907823(55)
q_{7J}	Hz	-13.646(11)
q_{7JJ}	uHz	43.37(57)

****

$v_6 = 1$

****

G_v	cm^{-1}	492.7605681(48)

x_{L66}	GHz	56.39
B_v	MHz	4229.25208(11)
D_v	kHz	0.462123(44)
H_v	mHz	0.0637(45)
L_v	nHz	-0.153
d_{JL66}	kHz	141.5
q_6	MHz	3.15095(11)
q_{6J}	Hz	-1.572(22)

****

$v_5 = 1$

****

G_v	cm^{-1}	522.2639330(49)
B_v	MHz	4225.835835(71)
D_v	kHz	0.452490(14)
H_v	mHz	0.03949
L_v	nHz	-0.153
q_5	MHz	2.68903(13)
q_{5J}	Hz	-1.627(27)

****

$v_7 = 2$

****

G_v	cm^{-1}	422.3753581(60)
x_{L77}	GHz	19.354043(61)
B_v	MHz	4247.45224(11)
D_v	kHz	0.491827(21)
H_v	mHz	0.03949
L_v	nHz	-0.153
d_{JL77}	kHz	-10.426(30)
q_7	MHz	5.93258(10)
q_{7J}	Hz	-13.897
q_{7JJ}	uHz	43.37

****

$v_7 = 3$

****

G_v	cm^{-1}	632.510162(64)
x_{L77}	GHz	19.1988(19)
B_v	MHz	4260.38118(15)
D_v	kHz	0.512469(34)
H_v	mHz	0.03949
L_v	nHz	-0.153
d_{JL77}	kHz	-10.947(24)
q_7	MHz	5.95888(12)
q_{7J}	Hz	-14.149(36)
q_{7JJ}	uHz	43.37

****

$v_5 = v_7 = 1$

****

G_v	cm^{-1}	734.058721(13)
x_{L77}	GHz	19.5125
x_{Lab}	GHz	23.13131(38)
r	GHz	0.32219(69)
r_J	kHz	-65.965(71)
B_v	MHz	4238.741823(94)
D_v	kHz	0.472594(28)
H_v	mHz	0.03949
L_v	nHz	-0.153
d_{JL77}	kHz	-9.971
d_{JLab}	kHz	-5.08(13)
q_a	MHz	2.70634(31)
q_{aJ}	Hz	-1.626
q_b	MHz	5.90943(72)
q_{bJ}	Hz	-13.738(97)
q_{bJJ}	uHz	43.37

****

$v_4 = 1$

****

G_v	cm^{-1}	867.594(74)
B_v	MHz	4212.271(16)
D_v	kHz	0.45312(11)
H_v	mHz	0.03949
L_v	nHz	-0.153

****

$v_6 = 2$

****

G_v	cm-1	983.021(77)
x_{L66}	GHz	56.39(57)
B_v	MHz	4236.558(15)
D_v	kHz	0.471993(61)
H_v	mHz	0.03949
L_v	nHz	-0.153
d_{JL66}	kHz	141.6(38)
q_6	MHz	3.15095
q_{6J}	Hz	-1.571

****

$v_6 = v_7 = 1$

****

G_v	cm-1	703.8550157(94)
x_{L66}	GHz	56.39
x_{L77}	GHz	19.3189
x_{Lab}	GHz	16.16651(21)
r	GHz	-17.04625(41)
r_J	kHz	-5.784(70)
B_v	MHz	4242.274182(82)
D_v	kHz	0.481887(24)
H_v	mHz	0.03949

L_v	nHz	-0.153
d_{JL77}	kHz	-11.254
d_{JL66}	kHz	141.5
d_{JLab}	kHz	43.88(12)
q_a	MHz	3.17827(15)
q_{aJ}	Hz	-1.571
q_b	MHz	5.94427(18)
q_{bJ}	Hz	-13.646
q_{bJJ}	uHz	43.37

****

$v_7 = 4$

****

G_v	cm^{-1}	841.9860892(94)
x_{L77}	GHz	19.03874(51)
y_{L77}	MHz	1.82(12)
B_v	MHz	4273.30576(21)
D_v	kHz	0.53448(11)
H_v	mHz	0.176(21)
L_v	nHz	-0.153
d_{JL77}	kHz	-11.368(21)
h_{JL77}	Hz	-0.0552(63)
q_7	MHz	5.98281(15)
q_{7J}	Hz	-14.288(46)
q_{7JJ}	uHz	43.37

****

$v_6 = 1, v_7 = 2$

****

G_v	cm^{-1}	914.21137(22)
x_{La}	GHz	56.39
x_{Lb}	GHz	19.1254(86)
x_{Lab}	GHz	16.2848(57)
r	GHz	-16.6526(81)

r_J	kHz	-12.0(12)
B_v	MHz	4255.2987(20)
D_v	kHz	0.502237(37)
H_v	mHz	0.03949
L_v	nHz	-0.153
d_{JLa}	kHz	141.5
d_{JLb}	kHz	-12.54(75)
d_{JLab}	kHz	43.75(46)
q_a	MHz	3.19092(19)
q_{aJ}	Hz	-1.571
q_b	MHz	5.9489(16)
q_{bJ}	Hz	-14.17(33)
q_{bJJ}	uHz	43.37

****

$v_5 = 1$, $v_7 = 2$

****

G_v	cm^{-1}	945.143633(31)
x_{Lb}	GHz	19.3142(16)
x_{Lab}	GHz	23.0216(30)
r	GHz	0.87043(33)
r_J	kHz	-64.05(11)
B_v	MHz	4251.64459(17)
D_v	kHz	0.492993(32)
H_v	mHz	0.03949
L_v	nHz	-0.153
d_{JLb}	kHz	-10.482(55)
d_{JLab}	kHz	-6.810(46)
q_a	MHz	2.72654(15)
q_{aJ}	Hz	-1.626
q_b	MHz	5.93169(23)
q_{bJ}	Hz	-13.646
q_{bJJ}	uHz	43.37

****

$v_5 = v_6 = 1$

****

G_v	cm^{-1}	1014.2947(11)
x_{L66}	GHz	56.39
x_{Lab}	GHz	40.245(33)
r	GHz	-63.498(66)
B_v	MHz	4233.55575(16)
D_v	kHz	0.463447(40)
H_v	mHz	0.03949
L_v	nHz	-0.153
d_{JL66}	kHz	141.5
d_{JLab}	kHz	80.35(29)
q_a	MHz	2.69091(31)
q_{aJ}	Hz	-1.626
q_b	MHz	3.15095
q_{bJ}	Hz	-1.571
u_{ab}	Hz	-1.641(73)

****

$v_3 = 1$

****

G_v	cm^{-1}	1968.328179(58)
B_v	MHz	4209.9044(17)
D_v	kHz	0.45297(37)
H_v	mHz	0.096(22)
L_v	nHz	-0.153

****

$v_2 = 1$

****

G_v	cm^{-1}	2252.138828(59)
B_v	MHz	4203.7900(20)
D_v	kHz	0.45509(49)

H_v	mHz	0.366(32)
L_v	nHz	-0.153

****

$v_1 = 1$

****

G_v	cm^{-1}	2608.518327(58)
B_v	MHz	4210.2179(18)
D_v	kHz	0.44988(41)
H_v	mHz	0.139(26)
L_v	nHz	-0.153

****

Resonance Parameters

****

C30(466)	$v_4 \sim 2v_6$	cm^{-1}	17.420(33)
C30(456)	$v_4 \sim v_5+v_6$	cm^{-1}	-6.527(13)
C50(47777)	$v_4 \sim 4v_7$	GHz	2.70065(75)
C50J(47777)	$v_4 \sim 4v_7$	kHz	9.807(35)

****

FIT STATISTICS:

****

file	no_of_lines	RMS error	weighted RMS
gs.lin	52	0.01327 MHz	0.8092
v7.lin	67	0.01095 MHz	0.7214
v6.lin	42	0.01713 MHz	0.7667
v5.lin	42	0.01371 MHz	0.6254
2v7.lin	61	0.02453 MHz	0.8607
v6v7.lin	93	0.03184 MHz	0.9258
v5v7.lin	78	0.02052 MHz	0.8432
3v7.lin	77	0.01981 MHz	0.7018

v4.lin	32	0.02338 MHz	0.8361
2v6.lin	54	0.04480 MHz	0.9411
4v7.lin	85	0.01977 MHz	0.7968
v6v7v7.lin	95	0.02186 MHz	0.9106
v5v6.lin	63	0.01501 MHz	0.7504
v5v7v7.lin	97	0.01738 MHz	0.8690
interstate.lin	10	0.01988 cm^{-1}	0.9942
nu7.lin	258	0.00005 cm^{-1}	0.9045
nu6.lin	267	0.00038 cm^{-1}	0.9443
nu5.lin	255	0.00037 cm^{-1}	0.9311
nu4.lin	109	0.00096 cm^{-1}	0.9615
nu6nu7.lin	166	0.00025 cm^{-1}	0.6236
nu5nu7.lin	170	0.00031 cm^{-1}	0.7685
nu5nu6.lin	102	0.00038 cm^{-1}	0.9562
2nu7.lin	136	0.00010 cm^{-1}	1.0436
2nu6.lin	141	0.00052 cm^{-1}	1.0386
3nu7-nu7.lin	208	0.00010 cm^{-1}	1.0226
nu4-nu6.lin	222	0.00005 cm^{-1}	1.0717
4nu7-nu6.lin	2	0.00004 cm^{-1}	0.8519
nu6-nu7.lin	309	0.00004 cm^{-1}	0.8973
nu5-nu7.lin	291	0.00006 cm^{-1}	1.1312
nu6nu7-2nu7.lin	402	0.00008 cm^{-1}	0.8319
nu5nu7-2nu7.lin	261	0.00011 cm^{-1}	1.1334
4nu7-2nu7.lin	302	0.00017 cm^{-1}	1.6580
2nu7-nu7.lin	391	0.00008 cm^{-1}	0.7880
3nu7-2nu7.lin	178	0.00008 cm^{-1}	0.7774
4nu7-3nu7.lin	89	0.00010 cm^{-1}	0.9787
nu6nu7-nu7.lin	329	0.00069 cm^{-1}	0.9246
nu5nu7-nu7.lin	464	0.00046 cm^{-1}	0.9148
nu6nu7nu7-nu7.lin	153	0.00047 cm^{-1}	0.9359
nu5nu7nu7-nu7.lin	296	0.00041 cm^{-1}	0.8260
2nu6-nu6.lin	43	0.00070 cm^{-1}	0.9358
nu5nu7nu7-2nu7.lin	106	0.00035 cm^{-1}	0.6942
nu6nu7nu7-2nu7.lin	93	0.00052 cm^{-1}	1.0469

nu3.lin	218	0.00032 cm^{-1}	0.7951
nu2.lin	199	0.00036 cm^{-1}	0.8914
nu1.lin	187	0.00035 cm^{-1}	0.8763

Overall weigthed RMS error: 0.9476

==========